SUBSURFACE CHARACTERIZATION OF THE PWALUGU MULTI PURPOSE DAM SITE USING

SHALLOW SEISMIC REFRACTION

TECHNIQUE

By

RICHARD K. KAFUI AKORLIE, BSc (Hons)

A Thesis Submitted to the Department of Physics,

Kwame Nkrumah University of Science and Technology

In partial fulfillment of the requirements for the degree

Of

MASTER OF PHILOSOPHY

College of Science

Supervisor: Dr. Akwasi Acheampong Aning

MAY, 2016

DECLARATION

I declare this submission is my own work towards the MPhil and that its content has no previously published materials by any other person except where it is duly acknowledged. It also contains no material accepted for the award of any other degree of the University.

RICHARD K.KAFUIAKORLIE	.....	26- 05- 2016
Student Name & ID	Signature	Date
(PG8045512)		

Certified by:

DR. AKWASI ACHEAMPONG ANING	.....	26-05- 2016
SupervisorName	Signature	Date

Certified by:

PROF. SILVESTER K. DANUOR	.....	26- 05- 2016
Head of Dept. Name	Signature	Date

ABSTRACT

2D shallow seismic refraction survey technique has been applied at the proposed Pwalugu dam site to find out how suitable the subsurface is, for the engineering project. The geology of the project site is made up of the Upper Voltaian which is mainly characterised by sandstone. Ten traverses having different lengths oriented across the strike with geophone separation of either 4 or 5 m were conducted at the site. Seismic data were collected using 10 Hz electromagnetic geophones with the ABEM Terraloc Mk.6, a 24 channel recording system. The data was processed with the ReflexW software into 2D velocity depth models unveiling three acoustic layers. P-wave velocities averaging up to1400,3200 and 5300m/s were recorded for the first, second and third layers respectively. The 2D velocity depth models together with geologic information from the study area reveal that the overburden is made up of alluvium, the intermediate layer is made up of compacted alluvial deposits whilst the third layer suggest the massive sandstone bed. The seismic method delineated the bedrock at depths greater than 20 m at thevarious locations.

TABLE OF CONTENTS

LIST OF TABLES

LIST OF FIGURES

LIST OF SYMBOLS *E* Young‘s modulus

σ Poisson‘s ratio

K Bulk modulus

μ Shear modulus

v_p P-wave velocity

v_s S-wave velocity

ρ	Density
τ	Shear stress
P	Volume stress

ACKNOWLEDGEMENTS

I wish to first acknowledge the Almighty God for the strength and protection He granted unto me since the beginning of the programme. To my loved ones such as my Parents, Emelda, siblings and friends; I wish to express that am grateful to you all for your support and encouragements.

My profound gratitude goes to my supervisor Dr. A. A. Aning, Prof. S.K Danuor and Mr. Amedufo for their guidance. All the following names are appreciated for their support during the course: Issahaku Jackalia Sontaa, Nathaniel Sackey, George Hinson, Obed Sedowua, Evans Quaye, Emmanuel Tetteh Huadji and Appiah Desmond. God richly bless you.

CHAPTER 1

INTRODUCTION

The area of geophysics involves the application of physical theories and measurements to find out the properties of the earth. This field dates to antiquity and mainly used in earthquake prediction. But major breakthroughs in geophysics began in the late 1500s with initial work in the areas such as gravity and magnetism (SEG, 2014).Geophysical techniques involve the study of the hidden parts of the earth using instruments to measure their physical properties. The measurements are mostly carried out from the earth surface and when the data is interpreted effectively, will give useful information about the subsurface such as faults and fractures.

Very important improvements in geophysical instrumentation in the early years of the 20th century has resulted in progress of geophysics and ultimately resulted in the theory of plates in the 1960s. Plates tectonic which study the interior structure of the Earth and the areas associated with global and regional processes are together known as Solid Earth Geophysics. Exploration geophysics which is a sub-discipline involves the use of geophysical theory and instrumentation to locate petroleum, aquifers and other resources.

Geophysics as a discipline has dramatically prepared man with the ability to exploit natural resources. For example, the variations in the Earth‘s gravitational field cannot be detected naturally by the human senses, but modern gravity meters can (in fact, to 0.02 parts per million or better).

Seismology which is mostly used for petroleum exploration utilizes the actual timing of very low amplitude vibrations moving through the earth and undetectable by the human senses (SEG, 2014).

Modern geophysical methods are used to map the subsurface and carryout geologic field reconnaissance surveys including the examination of in situ materials, man-made structures and water tables (Soupios et al., 2007). The most common geophysical methods include electrical, magnetic, gravitational, seismic, ground penetrating radar, electromagnetic methods etc.

The seismic technique relies on the travel times of sound waves, measured in milliseconds, travelling through the ground layers with contrasting acoustics properties. The seismic method has two techniques; seismic reflection and refraction, however this study employs the refraction technique. The method uses energy that flows through the subsurface and returns to the surface after travelling along ray paths to locate refractors that separate layers with different seismic velocities. The seismic refraction technique is a simple and effective means of obtaining valuable p-wave velocity information about a large volume of the subsurface material in two dimensions. P-wave velocity affects a number of geotechnical properties such as elastic and shear moduli, porosity and Poisson ratio.

Seismic refraction technique has been mostly used in groundwater and _contaminated site‘ investigations since it is relatively simple and it is adaptable for shallow zone investigations. Seismic refraction method detects groundwater as a boundary of acoustic impedance (Mooney, 1984).The possibility of using the seismic refraction method is determined by the elastic/acoustic properties of the near surface layers. The success of seismic refraction surveys in the determination of the thickness of weathered basement

and depths to water table has been very encouraging (Redpath 1973; Spencer 1973; Ushie 2010).

Though this method has limitations like hidden and thin layers (lower velocity layer sandwiched in high velocity layers), refraction seismic is capable of revealing significant information about the velocities of layers beneath the surface besides their thicknesses, elastic properties and water content when used in conjunction with exploratory drill. Refraction data can therefore strengthen the usefulness of exploration drill data (Rucker,- 2000; Dutta, 1984; Sjøgrenet al.,1979; Hatherly et al.,1986; Kilty et al.,1986; Moustafa et al., 2012).

Over the past decades in West Africa, the application of geophysical techniques in site investigations for civil engineering projects is gradually gaining roots. The use of geophysical techniques in geotechnical investigations has the capability to expose the subsurface image of a construction site which is very essential to the civil engineer (Goldstein, 2009; Benson et al., 1984; Benson and Yuhr, 1995; 2002). As a matter of fact the lack of sufficient knowledge about the subsurface strength distribution at a site before erecting a structure is in disguise a risk to the inhabitants and people living around such structures. Normally, questions pertaining to the foundation of buildings come to the fore when issues of buildings submerging under their load arise after some time.

Engineering geophysics reveals that the question of building foundation is frequently addressed in the very late stage when earthquake damage is either observed or expected (Delgado et al., 2000a, 2000b; Delgado et al., 2002; Ibs-von et al., 1999; Parolai et al., 2001, 2002).

Early detection of subsurface conditions that may pose potential danger to a building is crucial at the beginning and this can be accomplished with geophysical survey.

Undetected cavities, fissures and other near surface features such as high clay content can lead to foundation failure. Unfortunately, a lot of buildings are constructed on soils with insufficient bearing capabilities to support the weight of the structure. These soils may be partly made of clays which expand and shrink as the moisture content is changed and can cause the foundation of these buildings to respond resulting in unexpected breakdown from cracks if the moistening and drying of the clay is anomalous. Geological features and conditions beneath the surface such as voids, conduits, fractures, closeness of the water table to the surface, depth to bedrock etc. are some of the prominent threats to the foundations of structures (Andrews et al., 2013; Cecil,1971).

This approach has been successfully used at places with very hard rocks that have proven difficult to drill. It gives information on both the depth to bedrock and the quality of the hard rock (Rao et al., 2004). Shallow seismic refraction has been applied in the study of the properties of the bedrock in dam sites, road tunneling, quarries, nuclear power plants, hydroelectric power plants, subway construction, and many others. P and S- wave velocities obtained from shallow seismic refraction survey are used to estimate the depth to the bedrock and also determine its elastic properties. (El- Aal et al., 2010).

It must be admitted as a fact that lack of knowledge about the subsurface strength distribution at a site before erecting a structure is a risk to the inhabitants and the people living in the environment. Normally questions relating to the foundation of buildings come to the fore, when issues of buildings submerging under their load arise at a later time.

Surface geophysical studies such as seismic refraction is a prerequisite to obtaining a preliminary estimate of the deformation, shear strength, plasticity index, depth to bedrock and other petrophysical properties of the rock mass as well as the thickness of the overburden and weathered rock. The seismic refraction method has been applied to study these factors that can cause landslides, in addition to other geotechnical problems like compaction certification, evaluation of bearing capacity, earthquake site classification and subsidence investigation (Varnes, 1978).

The construction of a hydro-dam demands an understanding of the general geological setting of the proposed site. This provides information for the dam designers so they can accurately estimate the cost of the project. These investigations will help to answer questions like; what is the thickness of the overburden that must be removed to reach an acceptable foundation. What are the rock types that constitute the bedrock and to what extent are these affected by surface weathering. Whether the foundation is made up of faulting and jointing and to what extent is the permeability. What are the elastic properties of the foundation rock types, where can adequate supplies of construction materials like clay, sand, gravel and rock-fill be obtained within the vicinity of the dam site and finally, whether the excavated rocks could be reused in the construction of the dam embankment?. The results obtained from a geophysical study are required to give evaluation.

The purpose of such research is to give a general assessment of the suitability of the area for the intended project, thus how the structure should be designed. The results will also determine the types and extent of further investigations that must be conducted during the closing stages of the study or during design (Ueblacker, 2006). The seismic refraction is the most appropriate and frequently used method for investigating the proposed site for construction of multi-purpose dams.

1.1 Location of project site

The proposed site for the dam is located in the East Mamprusi District of Ghana(fig 1.1). The project area is located on the White Volta River about 15 km East of Pwalugu Bridge on the main Tamale- Bolgatanga road. The White Volta is bordered on the Southwest by the Gambaga escarpment (VRA Ghana, 2013). The district covers a total land area of 1,660 sq. km and lies in the interior woodland savannah belt.

Figure 1.1: Map of the proposed dam site (modified from VRA Ghana, 2013)

It is common to find grass vegetation with trees such as acacia, baobab and shea-nut trees. The grasses grow in tussocks and reach heights of three meters or more. The vegetation greatly depends on the prevailing climatic condition.

Two main types of soils can be found in the district, the savannah ochrosols and the groundwater laterite. The savannah ochrosols, which covers most parts the district, is moderately well drained and developed mainly on voltaian sandstone. The soil texture is loamy to sand with good water retention. The topography rolls with the Gambaga

escarpment, which marks the northern limits of the voltaian sandstone basin (East Mamprusi District, 2014).

1.2 Literature Review

Rao et al. (2004) investigated the bedrock at the site where a high rise reinforced cement concrete (RCC) bridge was being constructed across the Krishna river in the Nalgonda District of Andhra Pradesh- India. This survey was to locate the hard rock depth at three points in the center of the river where piers will be placed. Three seismic lines were used for the survey with a 24 channel signal enhancement seismograph. The seismic section revealed that the rock mass along the axis of the bridge had an undulating nature. The quality and strength was reasonably good with a minimum compressive strength of the hard rock at 70Mpa to 90Mpa.The top layer is more or less uniform but the second layer comprises of riverine material that which is swollen in the center of the alignment posing a problem for foundation design. Further results show a depression in the hard rock layer in the first line. The seismic section in the other two lines indicated that the depression was on the southern side of the third line and northern end of the second line.

The maximum depth of the channel was calculated at 24m along line_3, 27m along line_1 and 20m along line_2.They concluded that, the hard rock was found at 20, 27 and 18m and accordingly recommended that founding levels for these points are 50, 43 and 53m respectively.

Ilesanmi et al.(2013) at the Gurara Dam Phase II in northwestern Nigeria, used seismic refraction technique to study the area. The results were needed to assess the suitability of the area for the construction of the dam. Profile 2 revealed that, the velocities ranged from 183 to 6522m/s in the fresh bedrock. The overburden had velocities between 185 and 597m/s and its thickness was between 8.11 and 13.74m. The bedrock is characterized by

values ranging between 1000m/s and 1613m/s. The western end of the profile was observed to have a velocity of 787 m/s which he suspected to be a fractured basement rock.

Kilty et al. (1986) applied the seismic refraction technique at the Horse Mesa dam site. The purpose for the survey was to obtain more complete information about the bedrock properties. The team shot two long refraction lines along the axis of the existing roadway. Their result showed that the bedrock was highly irregular on the surface. The velocities ranged from 366 to 549m/s in the overburden rock and between 1829 and7620m/s below the overburden. The interpreted results were compared to seven core data done on the roadway and some significant amount of accuracy was observed. They recommended that the GRM was an effective interpretation method.

Bekler (2011) used the seismic refraction method together with electrical resistivity and hydrometer methods to characterize landslide in Adatep-Canakkale, NW Turkey. The survey was aimed at understanding the conditions that give rise to slope failures along the highway in that locality. In the seismic aspect of the survey, the profile length was 124 m and this line was placed parallel to the landslide axis that crosses the highway. The velocity variations were displayed on velocity cells (pixels) and the ray hit counts were produced. The hit counts plot showed the ray resolution map and defines which portion of the velocity image is most reliable.

In similar experiments Al Saigh et al. (2014) used the Seismic Refraction Tomography and Multi-Channel Analysis of Surface Waves, for geotechnical evaluation of soil at the Teaching Hospital project at Mosul University. The purpose of the survey was to delineate the engineering characteristics of the shallow soil for construction purpose. The study covered a total area of 35140 m^2. Their results indicated that, the upper layer had p- wave

velocity ranging between 340-700 m/s and a thickness of 0.0- 4.2 m. The middle layer had p-wave velocity ranging between 840- 1700 m/s and the thickness ranged from 4.7 to 18 m. The lower layer was characterized by p-wave velocity ranging between 1900- 2800 m/s. It was found that the density gradient and stress ratio of this layer ranged between (-0.6- 0.61) and (0.33- 0.32) respectively. The conclusion made was that, the engineering parameters indicated good competent third layer and therefore recommended it as the most eligible layer for foundation purposes. The team recommended seismic refraction tomography for subsurface investigations.

Khan (2013) combined the electrical resistivity and seismic refraction technique in order to have a pictorial model of the shallow subsurface in terms of main geological and geophysical properties covering the premises of the University of Peshawar (UOP) Khyber Pakhtunkhwa, Pakistan. The results obtained from the survey showed two- layers separated by a refractor which gently slopes. The compressional wave velocities of the layers are 223 and 316 m/s for the overlying and underlying layers respectively.

1.3 Problem statement

The current energy crisis which is affecting Ghana‘s economy in a negative way and there are calls for an urgent need for government to find alternative sources of energy. The river Volta at Pwalugu is an alternative source of generating hydroelectric power in the country if developed by government. The White Volta always overflows its banks anytime Burkina- Faso opens the Bagri dam causing damage to lives and properties. This reason calls for the need to construct a dam at Pwalugu so it can be used to control flooding.

Similarly, the inability of the area to experience regular rainfall which is a requirement for agricultural and domestic developments has brought hardships on the locals. These

reasons also calls for the need to site a dam at the location which will cut down the problems the people are facing.

The possibility and workability of the dam at Pwalugu in the Northern Region of Ghana depends on whether the site; is filled with sand or silt deposits, has permeable bedrock, faults and folds in the subsurface.

In view of the outlined problems above, there is the need to carry-out a geophysical study in order to find out if the area is suitable for the project.

1.4 Research objectives

Geophysical investigations are very important for most civil engineering works such as the construction of dams, skyscrapers, bridges, underground tunnels, etc. The primary objective of the geophysicist in site characterization is to investigate the subsurface and delineate possible features that can adversely affect the foundations of structures. A fair idea of the near subsoil geologic features at a site proposed for construction is essential for the civil engineer to lay the best of foundations and position a building appropriately.

Site investigations are usually carried out to determine geotechnical parameters that reflect the behaviour of the subsurface from the engineering point of view. Some parameters that are measured in geotechnical studies may include the seismic wave velocity, soil porosity, bulk density of rock, water saturation, shear modulus, poisson‘s ratio, bulk modulus etc. All these parameters are relevant in a geotechnical work to assess the suitability of a site for a particular structure. The primary role of the geophysicist in site investigation is to determine regolith thicknesses and elastic wave velocities which is a guide to the strength of rocks. Compact soils (normally volcanic soil) have low amount of pore spaces, high bulk density and elastic wave velocity.

The specific objectives are; investigating the subsurface and delineating possible features to ascertain if the foundation can support the dam. Calculate the respective layer seismic velocities, determining the thicknesses of the layers encountered, find the depth to the bedrock and its orientation and finally determining the elastic properties of the rock layers.

1.5 Thesis structure

The thesis work is comprised of six (6) chapters and each chapter is addressing a main heading.

Chapter one introduces the subject, outlines the background of the research, objectives, justification of the objectives of the research, location and accessibility of the research area, as well as the literature review. Chapter two throws more light on the overview of the geological setting of West Africa and Ghana as a whole. It reviews both the regional and local geology of the study area. Chapter three outlines the main fundamental theories and limitations of seismic refraction and enhancement techniques applicable to seismic data. Chapter four gives an overview of the field methodology used to acquire the datasets and the available software for enhancing the datasets. This chapter also outlines the processing steps employed during the data processing stage of this work. Chapter five analyses the various seismograms obtained from the survey with detailed interpretation. The final chapter outlines the conclusion made and the recommendations for future work.

CHAPTER 2

GEOLOGICAL SETTING

2.1 Regional Geology

2.1.1 The West Africa Craton

The West African Craton is one of the five large masses of the Precambrian basement rock of Africa that make up the African plate (Doblas et al., 2002). From the work of Begg et al. (2009) the West African Craton appears to have been formed by the three Archean Cratons, the Man-shield, Taoudeni and Reguibat as indicated in figure 2.1. The Man-shield and Taoudeni was believed to have come together around 2,100Ma and Reguibat Craton docked at around 2,000Ma. Their roots extended to about a depth of over 300km in the sub-continental lithosphere mantle.

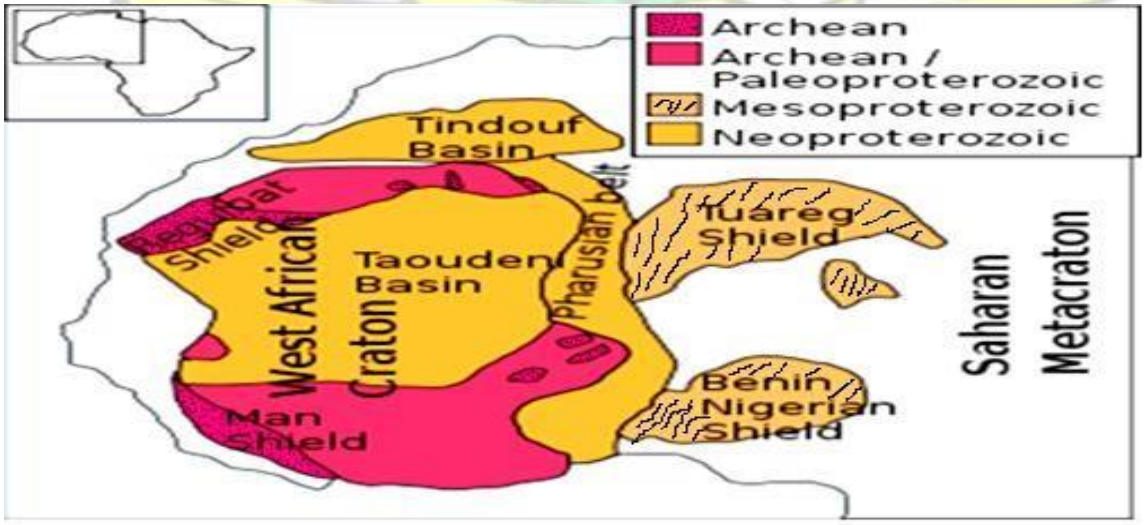

Figure 2.1: The West African Craton (en.wikipedia.org, 2010)

The West African Craton stabilized in the early Proterozoic (2000Ma) during the time of the Eburnean Orogeny. The Eburnean Orogeny also stabilized the Zaire Craton and vastly

affected parts of West Africa and neighboring regions in South America that were conterminous with Eburnean tectonothermal province.

In the West African Craton, lower Proterozoic rocks are extensively preserved. These rocks comprise of extensive belts of metamorphosed volcanic and sedimentary rocks exposed in countries such as Ghana, Burkina Faso, Niger and Cote d'Ivoire (Kesse, 1985).West Africa Craton is bounded to the east and west by late Proterozoic mobile belts (700-500Ma) which is also called the Pan African mobile belts (Wright, 1986; Leube, 1990).

The Man-Shield represents approximately 45% of the exposed geology of Ghana, being largely restricted to the northern, western and south- western portions of Ghana. The shield area is confined to the southeast by the Proterozoic Togo Mobile Belt and central- eastern portion is largely covered by late Proterozoic to early Paleozoic sedimentary rocks of the Volta Basin (Castle Minerals Pty Ltd, 2012).

2.2 Geology of Ghana

According to the Ghana Geological Survey (GGS) document (2009), Ghana is subdivided into four major distinct lithostratigraphic complexes as shown in figure 2.2.

2.2.1 Paleoproterozoic Supracrustal and Intrusive Rocks

The Paleoproterozoic supracrustal and intrusive rocks which were formed between 2195 Ma and 2072 Ma consist of the Birimian Supergroup, Tarkwaian Group (2134- 2118 Ma), Eburnean

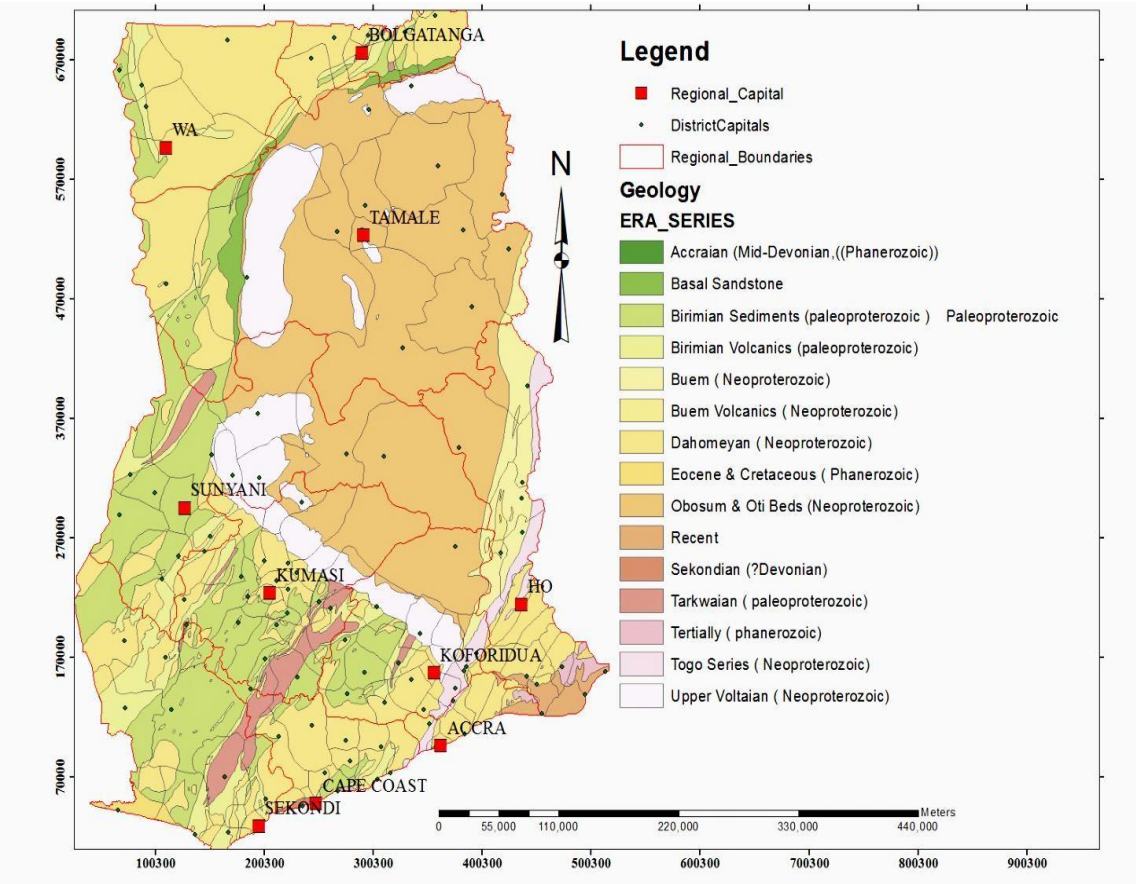

Figure 2.2: The four major distinct lithostratigraphic complexes/Era Series of Ghana (GGS, 2009)

Plutonic Suite (2116- 2072 Ma) and _Tamnean‘ Plutonic Suite (2134- 2118 Ma).

Most part of the Paleoproterozoic terrain of Ghana is underlain by intrusive and supracrustal rocks of the Birimian Supergroup and it displaces a NE-trending, approximately evenly- spaced and parallel _volcanic belts‘, and intervening _sedimentary basins‘. The _volcanic-belt‘ is called the Plutonic Group and the _sedimentary basins‘ are called the Sedimentary Volcano-Sedimentary Group. Rocks of the Volcano- Plutonic Group are lithologically and genetically diverse but most of the _volcanic-belts‘ rocks are dominantly made up of low grade metamorphic tholeiitic basalts with intercalated volcanoclastics and minor andesitic, felsic flow rocks and locally chemical sediments. The

volcanic rocks in this belt are intruded by coeval, comagmatic, and synvolcanic granitoid plutons.

The terrains in the Sefwi, Ashanti belts represent a tectonically stacked sequence of volcanic chains. Rocks of the sedimentary- volcano- group between the _volcanic belt‘ are low-grade metamorphosed, tightly to isoclinally folded sediments comprising volcaniclastic wackes and argillites. Depending on the relative abundance, these materials form different lithological group, the facies representing the different depositional paleo environments (GGS, 2009).

The Birimian Supergroup is made up of the Sedimentary-Volcano-Sedimentary Group, the Volcano-Plutonic Group (volcanic and synvolcanic intrusive rocks) and the Birimian Protoliths affected by Eburnean Tectonometamorphic over print. Some examples of these rocks are: chert/volcaniclastic sediment, dacitic to rhyolitic flow/hornblende biotite granite, and granitoid amphibolite/ biotite gneiss respectively(GGS, 2009).

The Tarkwaian Group consists of polymictic and quartz-pebble conglomerates, sandstones and minor argillites, siltstones and tuffs. It is present in some parts of the Brong- Ahafo and Eastern regions (GGS, 2009).

Eburnean Plutonic Suite is present in areas such as the Cape Coast basin, Kibi- Winneba belt, south of Kumasi basin, Suhum basin, Lawra belt and the Bole- Nangodi belt. It is composed of rocks such as biotite granite, hornblende-biotite tonalite, gabro, ultramafic and minor mafic igneous rock undifferentiated etc. (GGS, 2009).

The _Tamnean‘ Plutonic Suite is found in the Suhum basin, parts of the Upper East and Upper West and the western parts of the Northern Regions of Ghana. These areas consist

of rocks such as alkali granites, syenite, biotite- hornblende granite, biotite tonalite etc (GGS, 2009).

2.2.2 Neoproterozoic

2.2.2.1 Neoproterozoic to early Cambrian

According to a GGS report in 2009, the Neoproterozoic to Early Cambrian consist of the Dahomeyan and Voltaian Supergroups. The Voltaian Supergroup consist of the 1000 to 950 Ma old Kwahu-Morago Group at its base, followed after a hiatus of300 Ma by the Oti-Pendjari Group that was deposited around the same time the Dahomeyan was also forming (after 630 Ma).The late Neoproterozoic to Early Cambrian Obosum Group (younger than 547 Ma) is at the top.

Sedimentary rock of Volta Basin can be subdivided into three units. The Bombouaka Supergroup, the Oti-Panjari Supergroup and, the Tamale Supergroup. The thickness of the Bombouaka Supergroup is about 1000m and comprises mostly of sandstone and soft clay siliceous sediments. The Panjari Supergroup has an average thickness of approximately 2,500m and rests with an erosional unconformity partly of glacial origin on various Bombouaka rocks, or crystalline basement. Predominant rock types at the base include an association of tillitedolomitic limestone with baryte-silixite, and in the upper partrhythmic argillites and siltstones. The Tamale Supergroup has a thickness of about 500m and is made up of clay and siltstones in its lower part and sandy, coarser continental rocks at the surface. The Tamale Supergroup represents a typical forehand molasses basin.

The Bombouaka Supergroup is estimated to be between the ages of 1,100 and 700 Ma, and that of the Oti-Panjari Supergroup is about 700-600 Ma whereas the age of the

Tamale Supergroup is controversial because it is sometimes assigned to the upper Neoproterozoic to basal Cambrian or sometimes to the lower Paleozoic and thus could be time equivalent to the Sekondian and Accraian series developed along the coast of Ghana (Schlüter, 2006).

2.2.2.2 Pan African Mobile Belt

The Neoproterozoic Pan African mobile belt terrains of eastern and southeastern Ghana consist mainly of the Togo Series with quartzite, shale and minor Serpentinite, the Dahomeyan System comprising mafic and felsic gneisses, the Buem Group made up of shale, sandstone, basaltic to trachylitic lavas and volcanoclastics, the Kpassa complex and the Atacora complex comprising of Serpentinite, talc schist (GGS, 2009).

2.2.3 Phanerozoic Coastal Basin

The Phanerozoic rock units at several places along the coast include the Middle Devonian Accraian Group, the middle Devonian to lower Cretaceous Sekondian group, the upper Jurasic to lower Cretaceous Amisian Group, the upper cretaceous Apollonian Group and tertiary to recent unconsolidated marine, lagoonal and fluvial deposits(Schlüter, 2006).

The Phanerozoic coastal basins are believed to have formed after 542 Ma eraand consist of rocks such as the following;

Appollonian Group- limestone, marl, mudstone with intercalated sandy beds.

Sekondian Group – sandstone and interbedded shale.

Accraian Group – sandstone interbedded with shale.

Amisian Group – conglomerate, micaceous sandstone, arkose, mudstone etc.

Alluvial- Sand, silt and clay (GGS, 2009)

2.3 Geology of study area

The project siteis situated along the NW boundary of the East Mamprusi District of Ghana (figure 2.3). The Northern, NNW, SSW, Southern and SSE parts of the district is made up of the Obosum and Oti Beds.

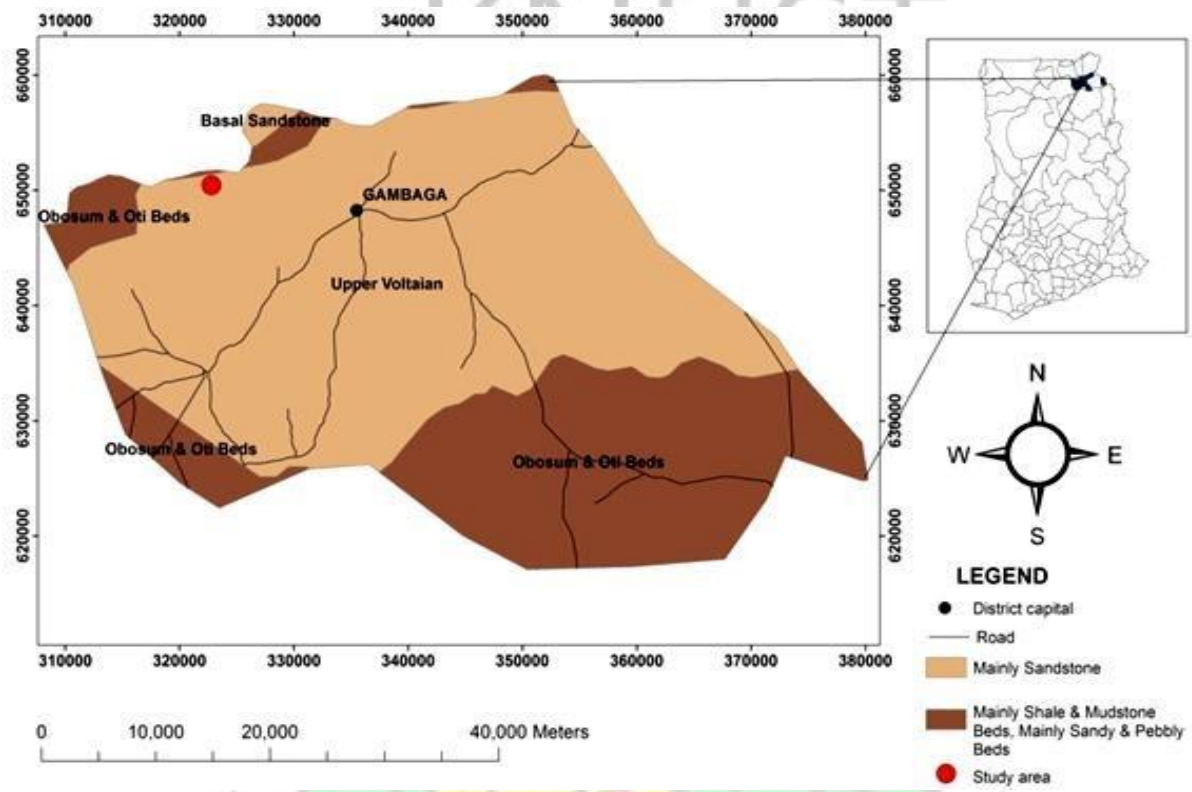

Figure 2.3: Geology of East Mamprusi district (GGS,2009)

The central portions, as well as the Eastern and Western parts are made up of the Upper Voltaian which is mainly sandstone. The Oti and Obosum beds are mainly shale and mudstone beds with some amounts of sandy and pebbly beds. The presence of basal sandstone can be seen around the NNE part.

CHAPTER 3

SEISMIC REFRACTION METHOD

This chapter reviews the seismic refraction principles. It also discusses some basic interpretation technique (intercept time method) and the limitations of this survey technique and their remedies.

3.1 Seismic refraction

3.1.1 Theory of elasticity

The method utilizes the propagation of acoustic waves through the earth. The wave propagation depends on the elastic properties of the rocks. The elasticity of a body is the property of resisting changes in shape and volume and returning to the original undeformed state when the external forces acting on it are removed. A perfect elastic body is one which completely recovers to its normal state after been deformed by a force. The theory of elasticity relates the applied forces to the resulting deformations using the concept of stress and strain.

Stress is the force per unit area. When a force acts perpendicular to a surface area, the stress is a normal stress and if the force is tangential to the area, it is referred to as a shearing stress. Any stress can be resolved into a normal or shearing stress. Strain is the relative change in the size and shape of a body subjected to a stressful force (Telford et al., 1990).

The linear relationship between the stress and the resulting strain on a material‘s elastic field is determined by the materials various elastic moduli. If we consider a rod with length (*L)* and cross sectional area (*A)* which is extended by a change ΔL resulting from an external force F applied to its end faces.

The Young's modulus *E* is expressed as;

$$\mathrm{E} = \frac{\text{longitudinal stress F/A}}{\text{longitudinal strain } \Delta\mathrm{L/L}} - - - - - - -(1)$$

The Poisson's ratio σ is given by;

$$\sigma = \frac{\text{lateral strain}}{\text{longitudinal strain}} - - - - - - - - - -(2)$$

The Bulk modulus K in the case of a simple hydrostatic pressure P applied to a cubic material is;

$$\mathrm{K} = \frac{\text{volume stress P}}{\text{volume strain } \Delta\mathrm{v/v}} - - - - - - - - - -(3)$$

The Shear modulus μ is given as;

$$\mu = \frac{\text{shear stress } \tau}{\text{shear strain } \tan\theta} - - - - - - - - - - - (4)$$

(Keary et al., 2002)

In terms of the compressional and shear wave velocities, the elastic constants are given as follows:

$$\mathrm{E} = \rho {v_s}^2 \frac{(3{v_p}^2 - 4{v_s}^2)}{{v_p}^2 - {v_s}^2} - - - - - - - - - - (5)$$

$$\sigma = \frac{\left[\left(\frac{v_s}{v_p}\right)^2 - 0.5\right]}{\left[\left(\frac{v_s}{v_p}\right)^2 - 1\right]} = \frac{({v_p}^2 - 2{v_s}^2)}{2({v_p}^2 - {v_s}^2)} - - - - - (6)$$

$$\mathrm{K} = \rho\left({v_p}^2 - \frac{4}{3}{v_s}^2\right) - - - - - - - - - - (7)$$

$$\mu = \rho {v_s}^2 - - - - - - - - - - - - - - - - - (8)$$

(Sheriff et al., 1995)

$$\rho = \alpha v_p^{0.25} \quad ----------(9)$$

(US Department of Transportation, 2014)

Where v_p is the P-wave velocity, v_s is the S-wave velocity, ρ is the bulk density and α is 0.31 when the velocity is in m/s

3.1.2 Body waves

These are waves which travel through the body of the medium. Two such waves are known. They are called the P wave and the S wave (fig 3.1b). P waves are also known as dilatational, longitudinal, irrotational or compressional waves. They are always the first to arrive in an earthquake. The second type is the shear, transverse or rotational waves. S waves are the second fastest to arrive at a detector. Unlike p-waves, the s-waves will never travel in pore spaces.

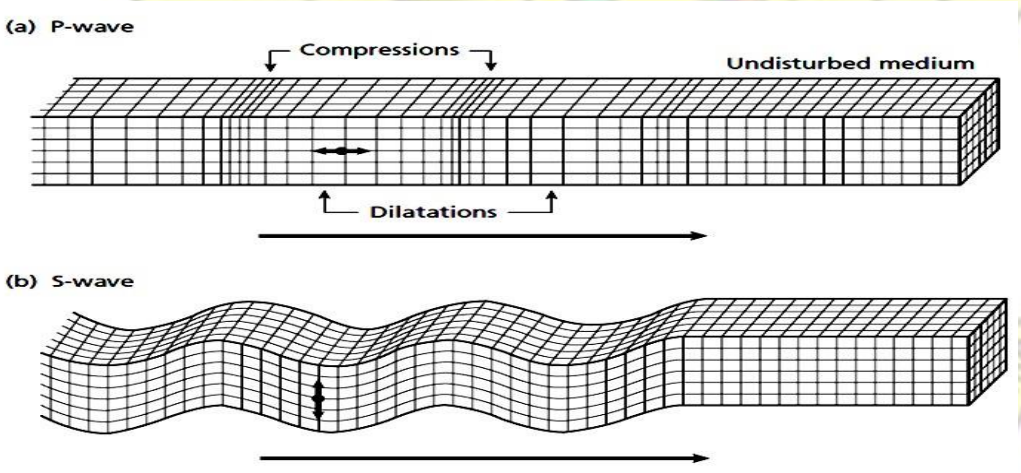

Figure 3.1: Elastic deformations and particle movements associated with body wavemovements

The velocities of p-waves (v_p) and s-waves (v_s) are given by equations 10 and 11

$$v_p = \left[\frac{K + \frac{4}{3}\mu}{\rho}\right]^{\frac{1}{2}} \quad ---------- \quad (10)$$

$$v_s = \left[\frac{\mu}{\rho}\right]^{\frac{1}{2}} - - - - - - - - - - - - - - (11)$$

Where the symbols have their usual meanings

The relationship between P wave and S wave velocities is given below as;

$$\frac{v_P}{v_S} = \sqrt{\frac{2(1-\sigma)}{(1-2\sigma)}} - - - - - - - - - (12)$$

Applying the nominal value of Poisson ratio for earth materials (σ~0.25) the relation in eqn. (12) becomes;

$$v_P \approx \sqrt{3} \times v_S - - - - - - - - - (13)$$

Two types of s- wave are of importance i.e. the Rayleigh wave and the Love wave (figure 3.2).Rayleigh waves also known as ground roll travel along the earth surface and is made up of longitudinal and transverse motions with a definite phase relation to each other. A love wave involves transverse motions that are parallel to the ground surface.

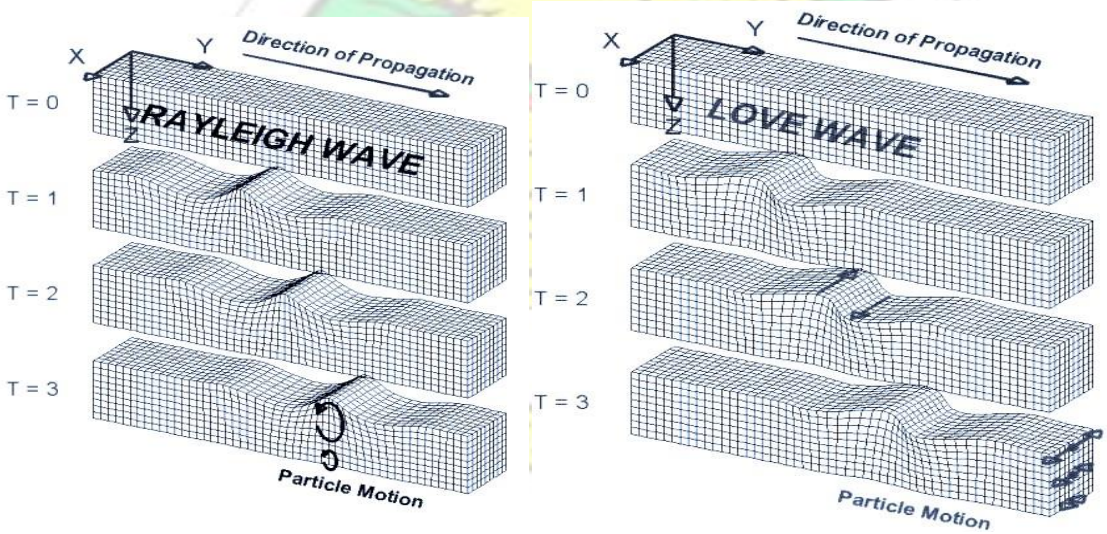

Figure 3.2: S-waves (scribd.com, 2013)

3.1.3 Sources of impulse energy in seismic refraction survey

According to Kearyet al.(2002) a seismic source is a localized zone within which a sudden release of energy leads to a rapid stress in the surrounding medium.

The major requirements of an energy source are;

- The energy source must be sufficient across the broadest possible frequency range up to the highest recordable frequencies.
- The energy source should be concentrated in the type of wave energy required for the survey.
- The source must be repeatable.
- The source must be efficient, safe and environmentally acceptable.

The source may be generated by explosive or non- explosive means like vibrators mounted on trucks, weight drops and hammers.

3.1.4 Seismometers

The seismometer detects the ground motion and converts it into electrical signals. Seismometers used in water based survey are called hydrophones and the land based seismometers are called geophones. The hydrophone detects the transient pressure changes caused by the passage of a compressional seismic wave. In the geophone however, there is a cylindrical coil suspended from a spring support in a magnetic field. As the waves pass through the ground, it causes a relative motion between the coil and the magnetic field produced by the magnet. The motion generates a voltage across the terminal of the coil as indicated in figure 3.3.

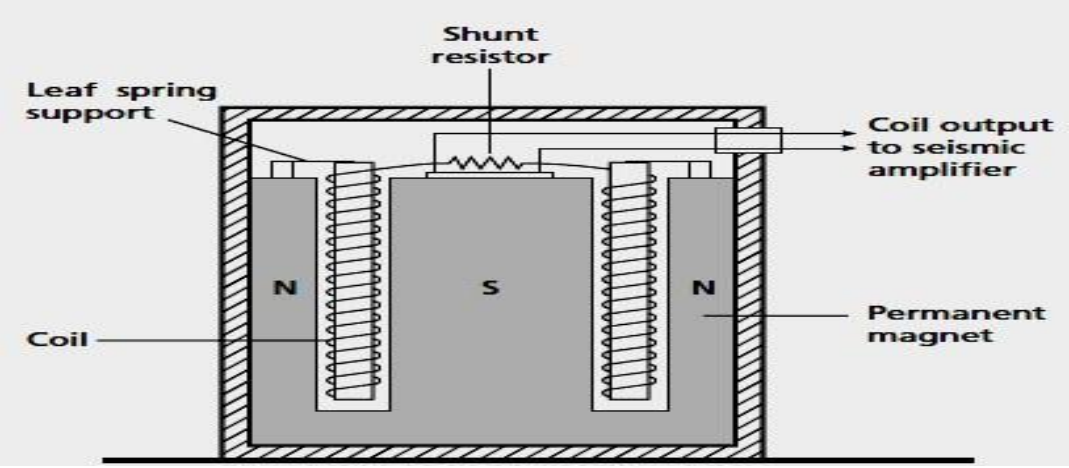

Figure 3.3: Cross- section through a moving coil geophone (Keary et al., 2002).

3.1.5 Shot detector configuration in seismic refraction survey

The shot detector setup can be done such that the shots will be fired at the mid-point between the geophone spread and this is called the split spread configuration or it can be setup so that the shots will be fired at the ends of the profile line (on- end spread) as shown in figure 3.4.

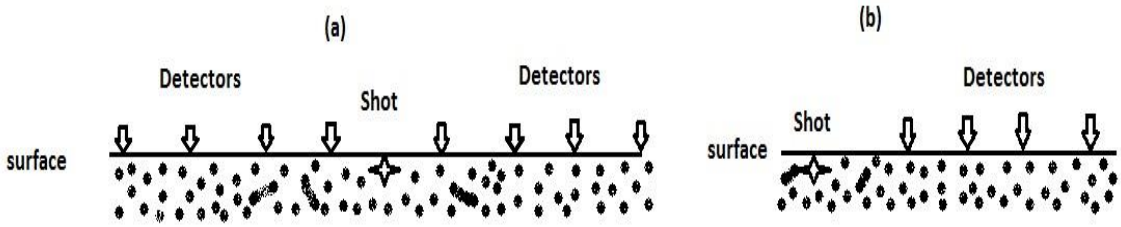

Figure 3.4: Shot detector configurations (a) split spread (b) on- end spread

3.1.6 Reverse shooting

This refers to the situation in which shots are taken at both ends of a profile line. The reverse shooting offers a significant advantage in the sense that, the true velocities and true layer thickness can be computed in details using the concept of delay time. When conditions are ideal, the depth to the refractor surface can be computed directly beneath each geophone to allow the mapping of irregular and dipping boundaries.

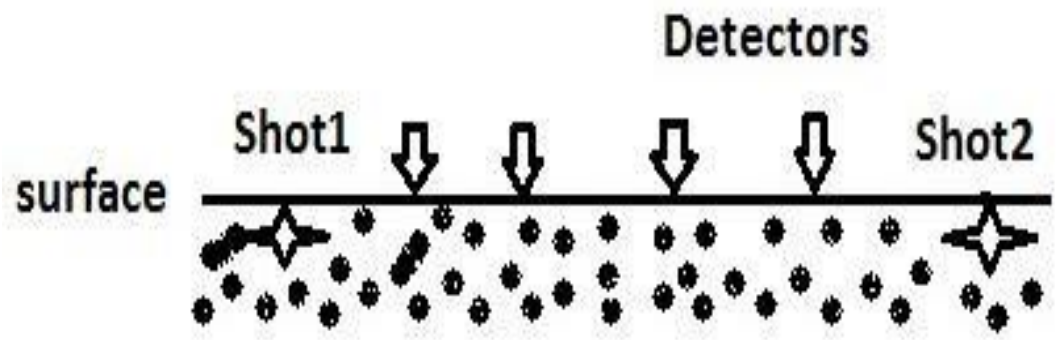

Figure 3.5: Concept of reverse shooting

3.2 Basic principles and theory

The method consists of measuring the travel times of compressional waves generated by an impulsive energy source. When seismic waves travel through the ground, they are refracted along boundaries between rocks with different acoustic impedance. The physical foundations of seismic refraction survey are Snell's Law and the phenomenon of critical incidence. Suppose seismic wave is moving through layered bodies with different acoustic impedance. Let the velocity of the top layer be $V_1$and V_2be the velocity of the underlying layer. At the interface, a wave is refracted or reflected depending on the elastic contrast measured by the change of acoustic impedance Z and the incident angle (eqn. 14).

$$Z = \rho V \quad (14)$$

where ρ is the density of the medium and V is the elastic velocity

It is difficult to relate acoustic impedance to a tangible rock property but, the harder a rock, the more the acoustic impedance. Intuitively, greater portion of the energy is transmitted through the interface if the contrast in acoustic impedance across the interface is smaller and the greater the contrast, the more the energy that is reflected. If the energy is incident at the interface at an oblique angle, the transmitted P-wave will travel through the layer below with a change direction of movement. This is called the refracted ray and Snell's law is applicable in this case.

At a certain critical angle of incidence, it is assumed that a critically refracted ray travels along the boundary between the two media at the velocity of the underlying layer. As the waves moves it continually generates seismic waves in the overlying layer and leaves the boundary as head waves with the same critical angle of incidence.

Snell‘s law states that: $$\frac{\sin i}{\sin r} = \frac{V_1}{V_2} - - - - - - - - - (15)$$

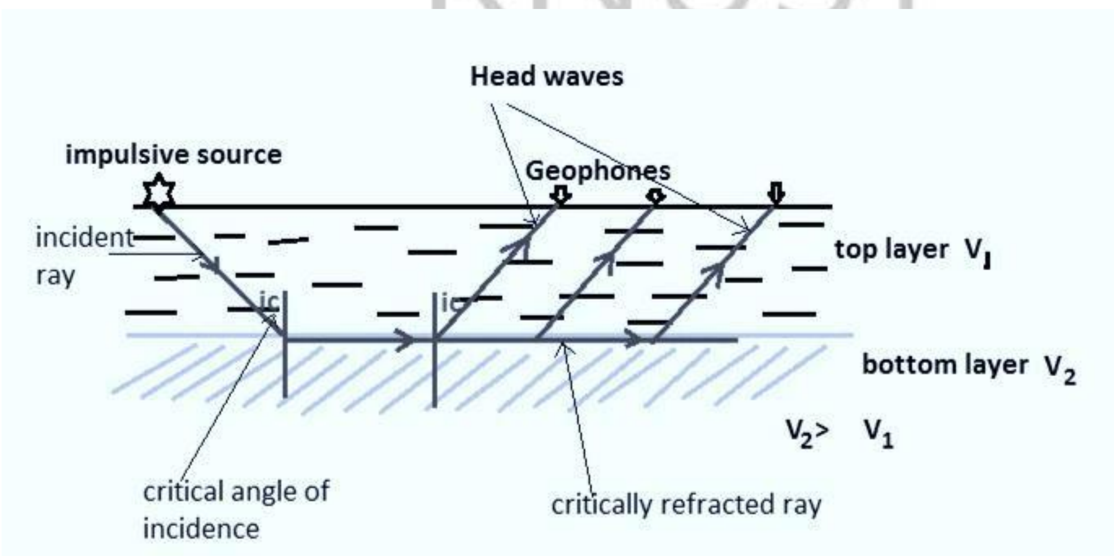

Figure 3.6: General ray path in seismic refraction

Where$i$and $r$are the angles of incidence and refraction respectively.

At the critical angle of incidence(i_c)as indicated in figure 3.6the refracted angle is 90° and the Snell‘s law becomes

$$\frac{\sin i_c}{\sin 90^\circ} = \frac{V_1}{V_2} - - - - - - - - - - - (16)$$

$$\sin i_c = \frac{V_1}{V_2} - - - - - - - - - - - -(17)$$

The head waves are detected by a series of geophones laid out on the surface in a straight line. The arrival times of the impulses are plotted against the corresponding shot- to-detector distances(Reynolds, 1997)

3.2.1 Travel time along a refracted ray path

The travel time t_n of a critically refracted ray along the top surface of the nth layer is given by;

$$t_n = \frac{X}{V_n} + \sum_{i=1}^{n-1} \frac{2Z_1 \cos \propto}{V_i} - - - - - - - - (18)$$

But

$$\propto = sin^{-1}\left(\frac{V_i}{V_n}\right) - - - - - - - - - - - - (19)$$

Where$\propto$is the angle of incidence,*i*represents the layer just above a refractor and *n* is the total number of layers under consideration, V is the seismic velocity of a layer; *X* is the source receiver distance andZ_1 is the thickness of the overlying layer.

Consider the two layer model in figure 3.7below;

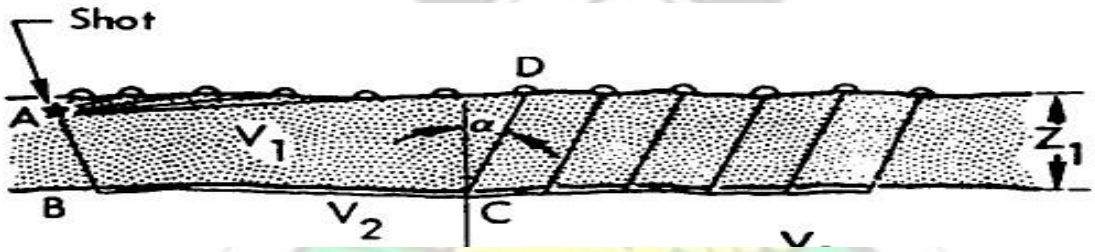

Figure 3.7: Schematics of a planar parallel boundary (Redpath, 1973).

The direct ray travels horizontally from A to D with a velocityV_1. The refracted ray travels from A to B at the velocityV_1, B to C at a velocity V_2 and then from C to D at a velocity V_1 .

The total travel time along the refracted ray path ABCD is the sum of the times from AB, BC and CD.

$$t = t_{AB} + t_{BC} + t_{CD} - - - - - - - - - - (20)$$

Therefore,

$$t = \frac{2Z_1 \cos \propto}{V_1} + \frac{X}{V_2} - - - - - - - - - - (21)$$

Where $\propto$ is $sin^{-1}\left(\frac{V_1}{V_2}\right)$ and X is the distance AD

3.2.2 Travel time curves

A travel time curve is a graph which shows the time it takes the seismic waves to travel from the source to a series of detectors placed at varying distances away.In other words, it is a plot of arrival times usually in milliseconds against the detector distances in meters. A travel time curve of a seismic survey indicates both the travel times of the direct wave, reflected wave and the refracted wave (figure 3.8).

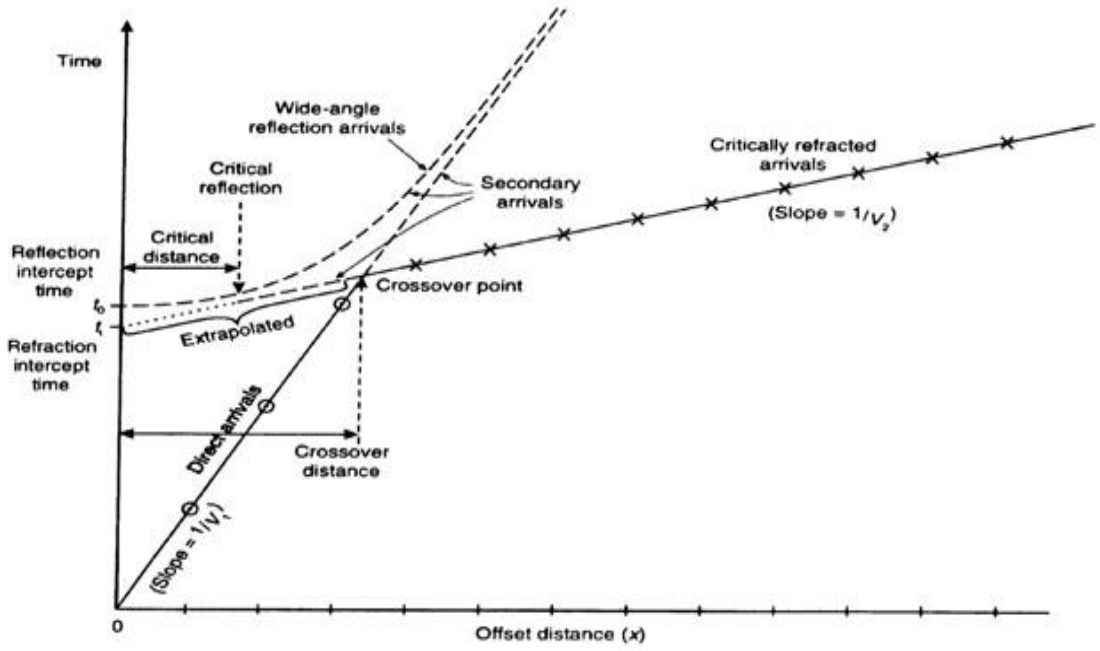

Figure 3.8: Travel time diagram indicating the paths for direct, reflected and refracted ray(Reynolds, 1997)

In refraction survey the refracted and direct ray arrival times are of importance. On the travel time curve for a refraction survey (figure 3.9), the velocity of the first layer is the reciprocal of the slope of the line indicating the direct- wave.

Because the travel time plot is a scatter diagram, the slope is given by equation (22)

$$\text{slope} = \frac{n\sum(xy) - \sum x \sum y}{n\sum(x^2) - \sum(x)^2} - - - - - - - - - - - (22)$$

where *x* is the offset, y is the arrival time and n is the number of data points

The velocity of the layeris the reciprocal of the slope of the line of best fit (eqn. 23).

$$\text{velocity (V)} = \frac{1}{\text{slope (m)}} - - - - - - - - - - - - (23)$$

When the straight line for the refracted arrivals is extended to the time axis, it intersects the axis at a time known as the intercept time (t_i) and it is given by equation (24)

$$\text{intercept time}(t_i) \ = \frac{\sum(y) - m\sum(x)}{n} - - - - - - - (24)$$

Where m denotes the gradient of the line of best fit and *x*, *y* and *n* have their usual meanings.

The distance from the shot point at which the head waves are detected first is called the critical distance (X_{crit}) and the distance at which the direct arrivals intersect the refracted arrivals is called the crossover distance (X_{cros}).

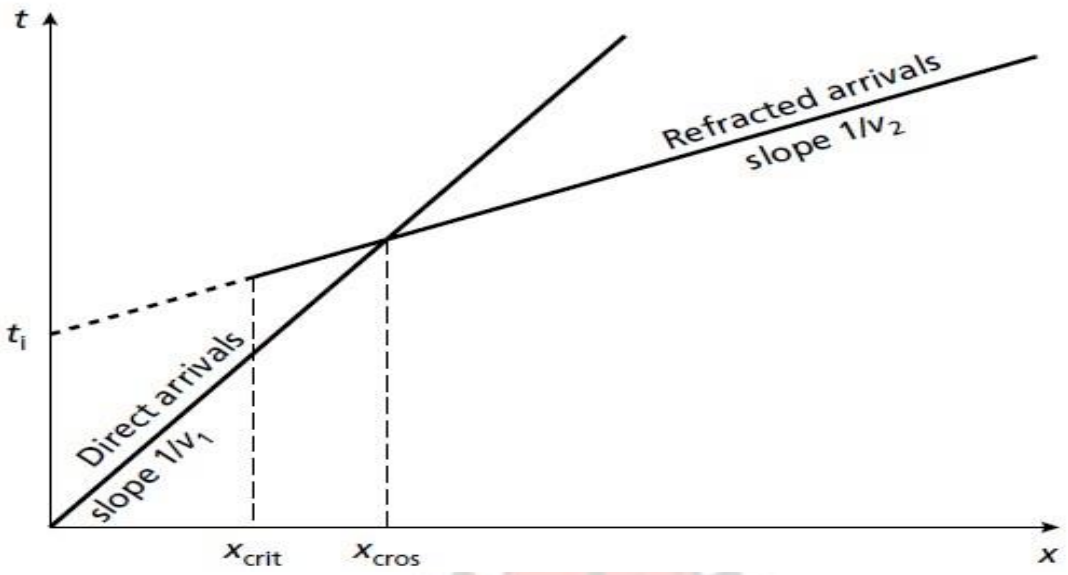

Figure 3.9: Travel-time curve of direct wave and head waves from a two layer model (Keary et al., 2002)

3.2.3 Acoustic properties of rocks

Rocks differ in composition, texture, porosity and contained pore fluids. As a result, they have different elastic moduli and densities and hence differences in seismic velocities. The P-wave velocities of rocks may be measured in situ by field measurement or done in the laboratory using suitably prepared samples. Dry rocks have their pore spaces filled with air and have low elastic velocity. Poorly consolidated rocks and disseminated soils may have strong adsorption of shear waves if they do not respond elastically (Milson, 2007). For very dry unconsolidated overburden, the p-wave velocity can be as low as 330 m/s (speed of sound in air) or less. The fluid contained poorly consolidated soils have velocity slightly greater than that of speed of sound in water (Milson, 2007). Therefore it is very important to recognize the effect of fluids on the velocity of materials. Furthermore, weathering also has a marginal reduction in the velocity of rocks and its pore content. This

condition reduces the rippability of rocks and it is of concern to the geotechnical engineer. Generally, the massive bedrock has p-wave velocity above 2500 m/s (Milson,2007).

The following empirical findings are very important to note:

- Compressional wave velocity increases when the confining pressure is increased.

 Increase in the depth of burial and age, increases systematically the velocities of sandstone and shale.

- The compressional wave velocity of a wide range of sedimentary rocks is related to density. Hence one can predict the densities of inaccessible layers using their seismic velocities.

- The elastic moduli, poison's ratio and V_p/V_s ratio are reduced by the presence of gas in sedimentary rocks. A ratio of V_p/V_s> 2 shows unconsolidated sand and a ratio of $V_p/V_s < 2$ shows either consolidated sandstone or a gas filled unconsolidated sand. (Keary et al.,2002)

The p-wave velocities (kms^{-1}) of some Earth materials are illustrated in table 3.1

Table 3.1 P - wave velocities of some materials (Keary et al., 2002)

Material	Velocity ($\mathrm{km}s^{-1}$)
Sand (Dry)	0.2 – 1.0
Sand (water saturated)	1.5 – 2.0
Clay	1.0 – 2.5
Permafrost	3.5 – 4.0
Sandstones	2.0 – 6.0
Tertiary sandstone	2.0 – 2.5
Pennant sandstone (carboniferous)	4.0 – 4.5
Cambrian Quartzite	5.5 – 6.0
Limestone	2.0 – 6.0
Cretaceous Chalk	2.0 – 2.5
Jurassicoolites and bioclasticlimestones	3.0 – 4.0
Carboniferous limestone	5.0 – 5.5
Dolomites	2.5 – 6.5

Salt	4.5 – 5.0
Anhydrite	4.5 – 6.5
Gypsum	2.0 – 3.5
Granite	5.5 – 6.0
Gabbro	6.5 – 7.0
Ultramafic rocks	7.5 – 8.5
Serpentinite	5.5 – 6.5
Air	0.3
Water	1.4 – 1.5
Ice	3.4
Petroleum	1.3 – 1.4
Steel	6.1
Iron	5.8
Aluminium	6.6

3.2.4 Geometry of seismic refraction ray path

The geometry looks at calculations involving the true velocity, perpendicular or vertical depth to refractor, the travel time of the ray etc. The subsurface is assumed to be composed of layers which are separated by planar and possibly interfaces that are dipping/irregular. Each layer is considered isotropic with regards to its velocity of propagation and the velocity of the seismic energy increases with layer depth.

Lastly the path followed by the ray is restricted to a vertical plane containing the profile line (Redpath, 1973).

3.2.4.1 Interpretation formulas (intercept time method)

3.2.4.1.1 The depth to a refractor with plane parallel interfaces.

Consider equation (21), if X=0, *t* becomes the intercept time t_i of the refractor layer. Therefore;

$$Z_1 = \frac{t_i V_1}{2\cos \propto} \quad ---------- (25)$$

But $\propto = \sin^{-1}\left(\frac{V_1}{V_2}\right)$ and t_i is read from the associated travel time curve. Hence

$$Z_1 = \frac{t_i V_1}{2\cos\left[\sin^{-1}\left(\frac{V_1}{V_2}\right)\right]} - - - - - - - - - - - - - - (26)$$

The true depth to the refractor according to Redpath (1973) is given by the sum of Z_1 and half the shot depth.

i.e.

$$Z_1 = \frac{t_i V_1}{2\cos\left[\sin^{-1}\left(\frac{V_1}{V_2}\right)\right]} + \frac{1}{2}\text{shot depth} - - - - - (27)$$

3.2.4.2 Multiple layers with plane- parallel boundaries

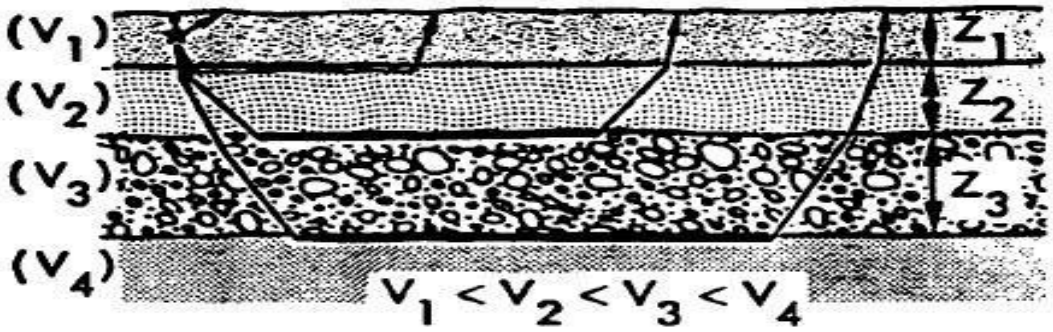

Figure 3.10: Schematic model of multiple layers with plane- parallel boundaries

(Redpath, 1973)

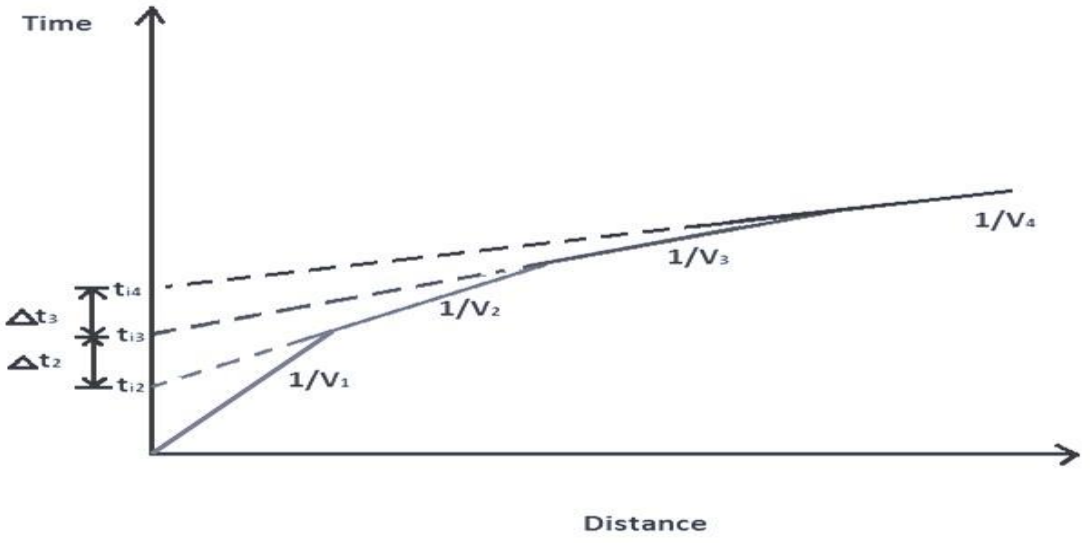

Figure 3.11: Travel-time curve of direct wave and head waves from a multiple layer model

The thicknesses of the second layer (Z_2) and the third layer (Z_3) are given by;

$$Z_2 = \frac{\left[t_{i3} - t_{i2}\dfrac{\cos\left(sin^{-1}\left(\frac{V_1}{V_3}\right)\right)}{\cos\left(sin^{-1}\left(\frac{V_1}{V_2}\right)\right)}\right]V_2}{2\cos\left(sin^{-1}\left(\frac{V_2}{V_3}\right)\right)} \quad \text{---------- (28)}$$

$$Z_3 = \left[t_{i2} - t_{i2}\frac{\cos\left(sin^{-1}\left(\frac{V_1}{V_4}\right)\right)}{\cos\left(sin^{-1}\left(\frac{V_1}{V_2}\right)\right)} + \frac{2Z_2\cos\left(sin^{-1}\left(\frac{V_2}{V_4}\right)\right)}{V_2}\right].\frac{V_3}{2\cos\left(sin^{-1}\left(\frac{V_3}{V_4}\right)\right)} \quad \text{--(29)}$$

(Redpath, 1973)

3.2.4.3 Determination of the dip angle, true velocity and the vertical distances to the refractor beneath the geophones in a dipping layer model

The best method of dealing with dipping refractors is to perform a reverse shooting during the experiment. The true refractor velocities can be properly determined by performing reverse shooting (Keary et al., 2002). When a dipping refractor arises along a profile, the

travel-time plots for the forward and reverse direction differ in gradient and intercept times.

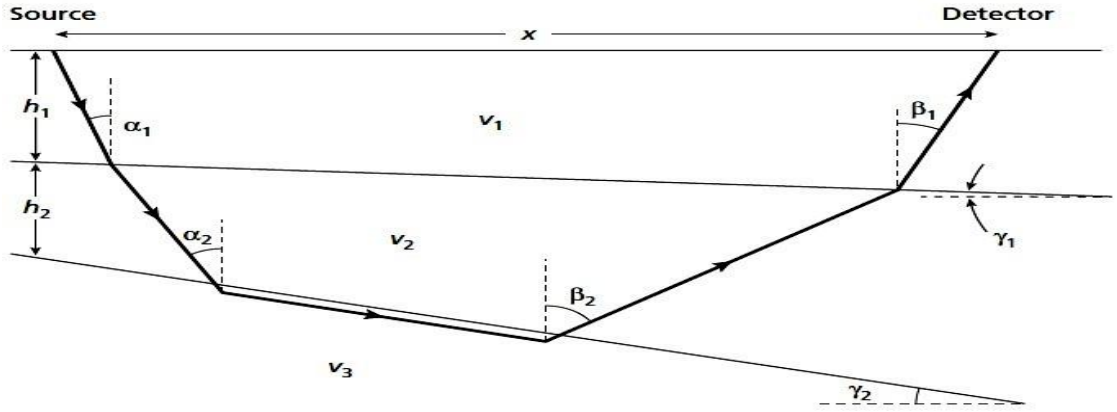

Figure 3.12: Refracted ray paths through a multi- layered dipping model (Keary et al., 2002)

The general equation for the travel-time $t_n$of a ray critically refracted on the surface of an *nth* dipping interface according to Keary et al.(2002)is given by;

$$t_n = \frac{X \sin \beta_1}{V_1} + \sum_{i=1}^{n-1} \frac{h_i(\cos \propto_i + \cos \beta_i)}{V_i} - - - - - (30)$$

h_i Correspond to the vertical thickness of the *ith* layer beneath the shot point.

$\propto_i$Is the angle made with respect to the vertical by the downward going ray in the *ith* layer.

β_i Represents the angle with respect to the vertical made by up going ray in the *ith* layer.

$V_i$is the velocity of ray in the *ith* layer.

*X*is the offset distance between the source and the detector.

$$\propto_i = \theta_{in} - \gamma_i - - - - - - - - - - - - - - - - - - (31)$$

$$\beta_i = \theta_{in} + \gamma_i - - - - - - - - - - - - - - - - - - - (32)$$

θ_{in}Is the critical angle of incidence when moving from an *ith* layer and γ_i is the dip angle of the *ith* layer.

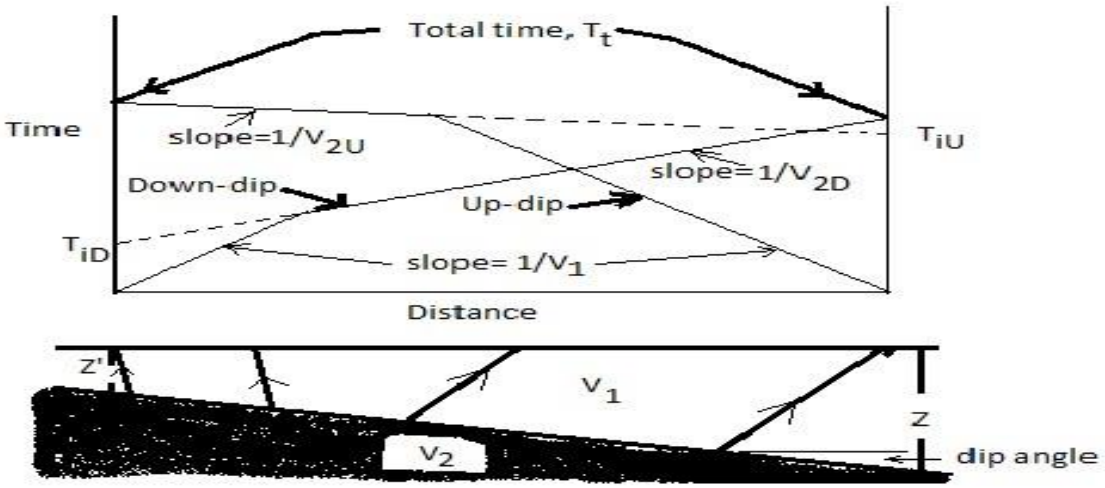

Figure 3.13: Schematic model of a dipping interface and the concept of reverse shooting and "apparent velocity:"(Redpath, 1973).

From figure 3.13, the apparent velocity of the refractor in the down dip direction is V_{2D} and from Snell's law

$$V_{2D} = \frac{V_1}{\sin(\theta_{12} + \gamma)} \text{----------(33)}$$

Similarly in the up dip direction, the apparent velocity is V_{2U} and from Snell's law it is given by

$$V_{2U} = \frac{V_1}{\sin(\theta_{12} - \gamma)} \text{----------(34)}$$

Where γ is the dip-angle

Rearranging equations (33) and (34) gives equations (35) and (36) respectively;

$$\theta_{12} + \gamma = sin^{-1}\left(\frac{V_1}{V_{2D}}\right) \text{----------(35)}$$

And

$$\theta_{12} - \gamma = sin^{-1}\left(\frac{V_1}{V_{2U}}\right) \text{----------(36)}$$

Equation (35) minus Equation (36) gives

$$\gamma = \frac{1}{2}\left[sin^{-1}\left(\frac{V_1}{V_{2D}}\right) - sin^{-1}\left(\frac{V_1}{V_{2U}}\right)\right] \text{-------(37)}$$

The true velocity $V_2$of the refractor is the harmonic mean of V_{2U} and V_{2D} multiplied by the cosine of the dip angle. (Redpath, 1973)

i.e.

$$V_2 = \frac{2V_{2U}V_{2D}}{V_{2U} + V_{2D}} \cos\gamma \quad ---------- (38)$$

As shown in figure 3.13,perpendicular Z and $Z'$to the interface under the two ends of the profile are obtained from the intercept time T_{iU} and $T_{iD}$of the travel time curves obtained in the forward and reverse directions.

$$T_{iU} = \frac{2Z\cos\theta_{12}}{V_1} \quad ---------- (39)$$

Therefore

$$Z = \frac{V_1 T_{iU}}{2\cos\theta_{12}} \quad ---------- (40)$$

Similarly

$$Z' = \frac{V_1 T_{iD}}{2\cos\theta_{12}} \quad ---------- (41)$$

By using the computed γ value, the perpendicular depths in equations 40 and 41can be converted into vertical depths h andh' respectively using;

$$h = \frac{Z}{\cos\gamma} \quad ---------- (42)$$

$$h' = \frac{Z'}{\cos\gamma} \quad ---------- (43)$$

3.2.4.4 Layers with non-planar interfaces

To investigate non-planar interfaces, the reverse shot is performed so that the depth to the refractor beneath each geophone can be mapped using the delay time method.

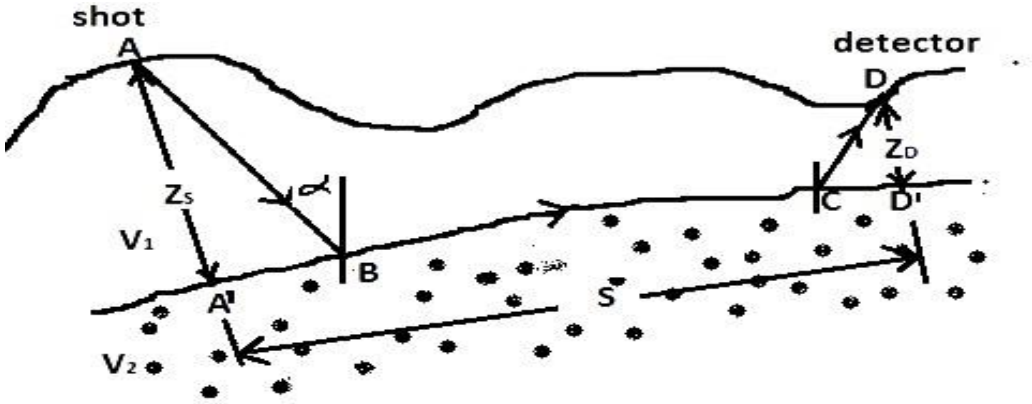

Figure 3.14: Non planar interface and definition of delay time

In figure 3.14, the expressions for the delay time at the shot point ΔT_S and the delay time at the detector ΔT_D are defined in equations (44) and (45) respectively below;

$$\Delta T_S = \frac{AB}{V_1} - \frac{A'B}{V_2} \quad ----------(44)$$

$$\Delta T_D = \frac{CD}{V_1} - \frac{CD'}{V_2} \quad ----------(45)$$

But $CD = \frac{Z_D}{\cos\propto}$ and $CD' = Z_D \tan \propto$, therefore

$$\Delta T_D = \frac{Z_D}{V_1 \cos \propto} - \frac{Z_D \tan \propto}{V_2} \quad ----------(46)$$

But $sin\propto = \frac{V_1}{V_2}, and\ V_2 = \frac{V_1}{\sin\propto}$ hence

$$\Delta T_D = Z_D \left(\frac{1}{V_1 \cos \propto} - \frac{sin^2 \propto}{V_1 \cos \propto} \right) ----------(47)$$

$$\Delta T_D = Z_D \left(\frac{1 - sin^2 \propto}{V_1 \cos \propto} \right) ----------(48)$$

$$\Delta T_D = Z_D \left(\frac{cos^2 \propto}{V_1 \cos \propto} \right) ----------(49)$$

But $\propto = sin^{-1}\left(\frac{V_1}{V_2}\right)$ therefore

$$\Delta T_D = \frac{Z_D}{V_1} \cos\left(sin^{-1}\left(\frac{V_1}{V_2}\right)\right) ----------(50)$$

Making Z_D the subject gives

$$Z_D = \frac{\Delta T_D V_1}{\cos\left(sin^{-1}\left(\frac{V_1}{V_2}\right)\right)} - - - - - - - - - - - - - (51)$$

If the value of the delay time at the detector $\Delta T_D$is known, then thedepth to the refractor beneath the geophone can be calculated.

From the same figure, the total delay time$\Delta T_{SD}$is given by;

$$\Delta T_{SD} = T_t - \frac{S}{V_2} - - - - - - - - - - - - - - - - - (52)$$

Where T_t is the total travel time from shot to the detector

The total delay time is the sum of the delay times at the shot and detector points. i.e.

$$\Delta T_{SD} = \Delta T_S + \Delta T_D - - - - - - - - - - - - - - - (53)$$

Hence

$$T_t - \frac{S}{V_2} = \Delta T_S + \Delta T_D - - - - - - - - - - - - - - (54)$$

Making ΔT_D the subject results in

$$\Delta T_D = T_t - \frac{S}{V_2} - \Delta T_S - - - - - - - - - - - - - - (55)$$

If the value of ΔT_S is known,ΔT_D and the depth to the refractor$Z_D$beneath the detector can be calculated.

Though the depth to the refractor surface below the shot point and the velocities of the layers are not known beforehand, we can still calculate the delay time beneath the geophone by firing shots at both ends of the line.

Consider the travel time curves for a reversed shot experiment (figure 3.15), the total travel times in the forward/ reverse shot are marked (T_t). The value of the total travel times should be the same for both shots.

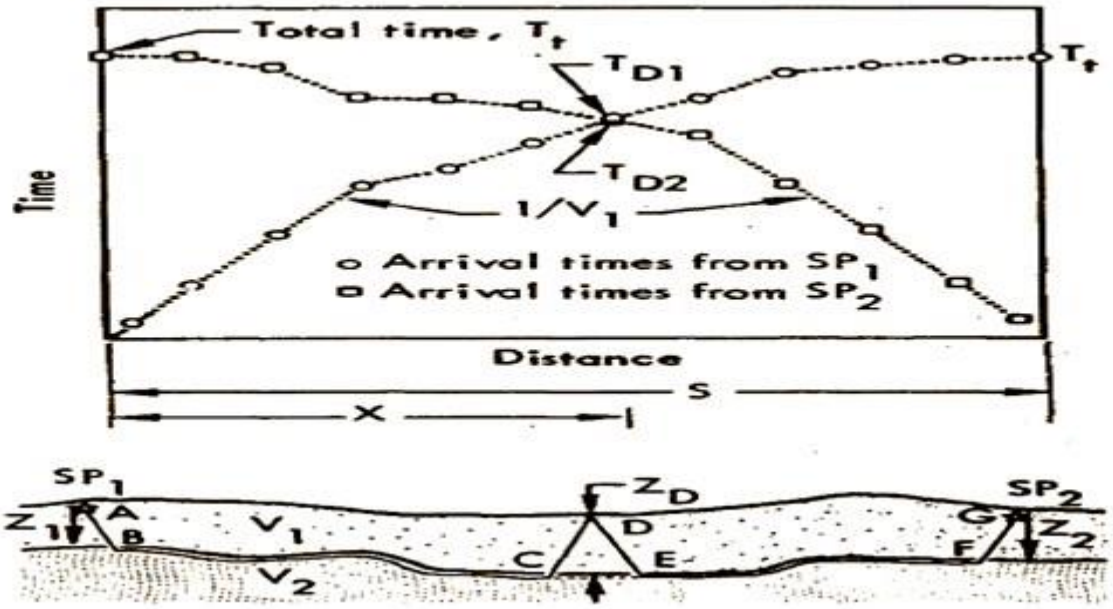

Figure 3.15: Delay time method of determining refractor depths at each geophone (Redpath, 1973)

The arrival time at a geophone from the two shots SP_1 and SP_2 has been marked as T_{D1} and T_{D2} respectively.

Using the equation (54), the total arrival times T_t can be expressed as;

$$T_t = \Delta T_D + \frac{S}{V_2} + \Delta T_S \text{ - - - - - - - - - - - - - - - - (56)}$$

Each arrival time can be written in terms of the component delay times. i.e.

$$T_{D1} = \Delta T_{S1} + \Delta T_D + \frac{X}{V_2} \text{ - - - - - - - - - - - - - - - - (57)}$$

$$T_{D2} = \Delta T_{S2} + \Delta T_D + \frac{S - X}{V_2} \text{ - - - - - - - - - - - - - - (58)}$$

Adding equations (57) and (58)

$$T_{D1} + T_{D2} = \Delta T_{S1} + \Delta T_{S2} + 2\Delta T_D + \frac{S}{V_2} \text{ - - - - - (59)}$$

But

$$T_t = \Delta T_{S1} + \Delta T_{S2} + \frac{S}{V_2} \text{ - - - - - - - - - - - - - - - - (60)}$$

Hence

$$\Delta T_D = \frac{1}{2}(T_{D1} + T_{D2} - T_t) - - - - - - - - - - - - - (61)$$

The depth to the refractor surface beneath the geophone is given by

$$Z_D = \frac{\Delta T_D V_1}{\cos\left(\sin^{-1}\left(\frac{V_1}{V_2}\right)\right)} - - - - - - - - - - - - - - - (62)$$

3.3 Limitations

3.3.1 The blind zone and velocity reversal

A blind zone refers to the case where there is a possible existence of a hidden layer resulting from the inability of the seismograph to interpret the existence of certain beds. This situation is usually caused by insufficient velocity contrast. The issue of ―blind zone‖ cannot be resolved by just changing the geophone layout and it is probably the greatest obstacle in the refraction method (Redpath, 1973).If the velocity contrast between the first and second layers is very large as illustrated in the figure 3.16 below, then a blind zone might be suspected. If a blind zone is not found out, then the error in the results would be a shallow computed depth to the surface of the refractor (Redpath, 1973).

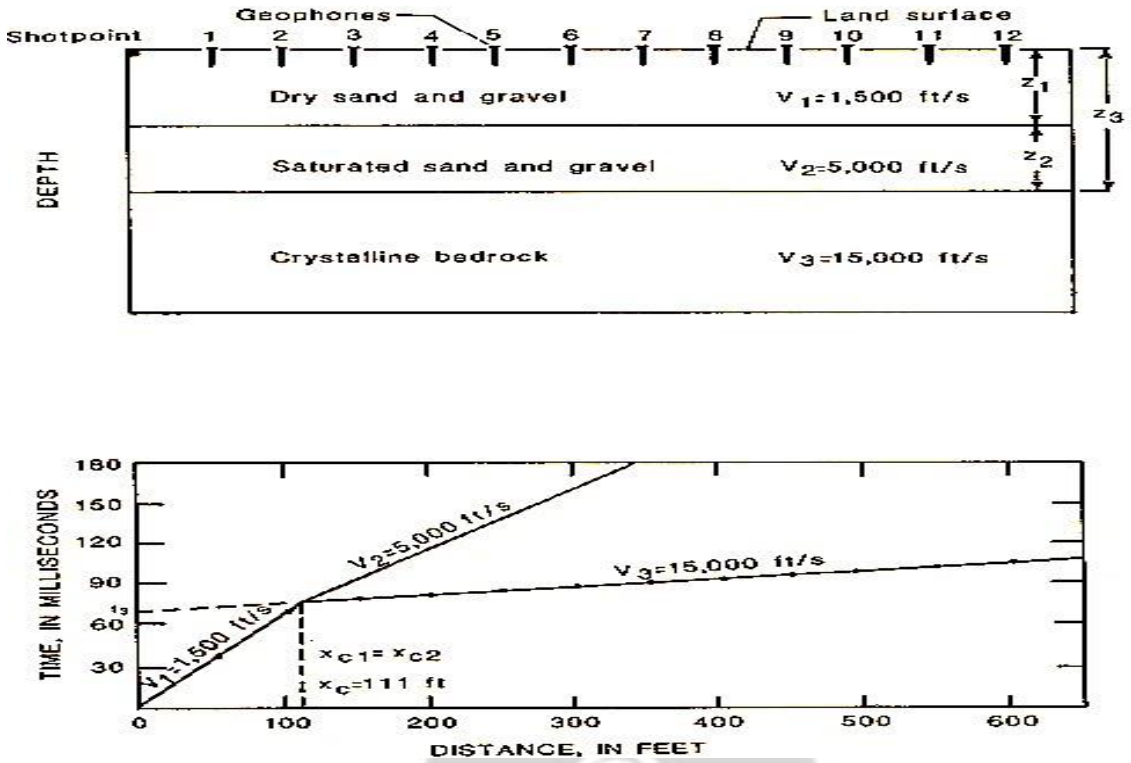

Figure 3.16: Seismic section with hidden layer problem and its time-distance plot (Haeni, 1988)

3.3.2 Minimum and maximum thickness of undetectable intermediate layer

Let Z_1 be the calculated depth from the time distance curve ignoring the possibility of an intermediate layer. According to Redpath, (1973) if the blind zone exists, there will be an infinite numbers of combinations of Z_1 and $Z_2$with Z_2mostly ranging up to its maximum, undetectable thickness at which Z_1 will be a minimum.

Let Z_{12} denote the thicknesses of the first two layers put together.

Therefore the minimum value of Z_{12} is given by

$$Z_{12}(min) = Z_1(max) + 0 - - - - - - - - - - - (63)$$

The maximum value of Z_{12} is given as;

$$Z_{12}(max) = Z_1(min) + Z_2(max) - - - - - - - (64)$$

Where Z_2 (*max*) is the maximum undetectable thickness of the second layer Z_1(*max*) is the value$Z_1$from the travel time curve.

Each quantity is determined with the formula below

$$Z_2(max) = \frac{RS}{R+S} Z_1(max) - - - - - - - - - - (65)$$

$$Z_1(min) = \frac{Z_2(max)}{R} - - - - - - - - - - - - - - (66)$$

Where

$$R = \frac{Z_2}{Z_1} \; and \; S = \frac{\tan \propto_{23}}{\tan \propto_{12}}$$

$$\propto_{12} = \sin^{-1}\left(\frac{V_1}{V_2}\right)$$

$$\propto_{23} = \sin^{-1}\left(\frac{V_2}{V_3}\right)$$

$$\propto_{13} = \sin^{-1}\left(\frac{V_1}{V_3}\right)$$

The *R* is determined by finding the intersection between $\propto_{12}$and $\propto_{23}$values and then interpolating between *R*- lines on a Nomograph (fig 3.17).

Due to the hidden layer problem it is always advisable to make seismic interpretations in conjunction with exploratory drill.

Velocity reversal occurs when a low velocity layer underlies a high seismic velocity unit. The occurrence of this phenomenon causes the low velocity layer to be undetectable. This occurs because from Snell's law, the waves are refracted downwards and the waves therefore will not be detected at the surface until it encounters a higher velocity layer. This is demonstrated in fig 3.18.

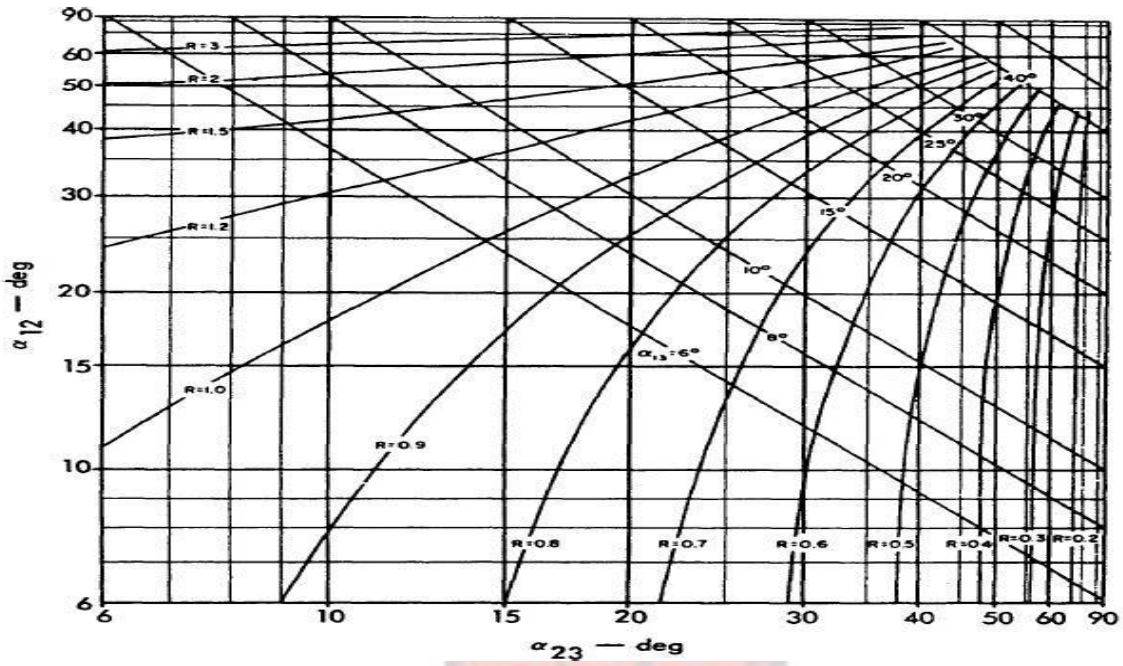

Figure 3.17:Anomographfor determining the maximum thickness of hidden layers (Redpath, 1973)

Some examples of this situation according to Haeni, (1988) includes; (1) unconsolidated sand and gravel aquifer underlying compact glacial tills. (2) Semi-consolidated rubble zones beneath dense basalt flows and (3) dense limestone overlying a poorly cemented sandstone.

If a low velocity layer is known to exist from a drill-hole data, then the estimated depths of the layers and the approximated velocities can be used to calculate the depth to the deeper refractor.

In the absence of a drill data, the calculated depth from the seismic section will be larger than the actual depth.

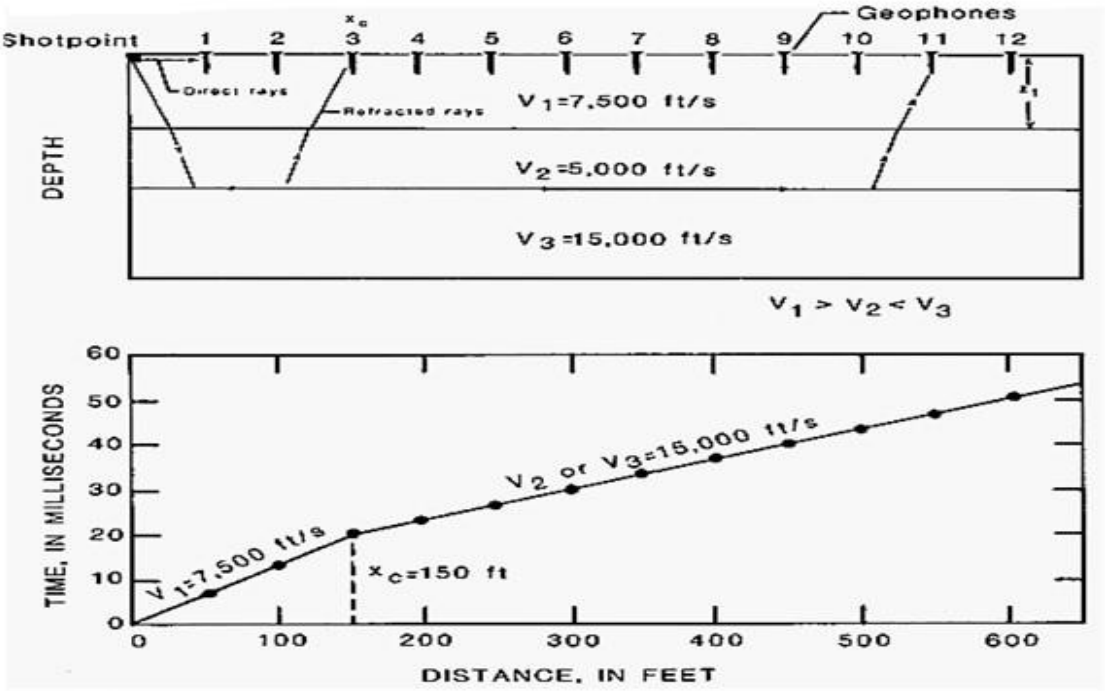

Figure 3.18: Seismic section with velocity reversal and resulting time-distance plot. (Haeni, 1988)

CHAPTER 4

METHODOLOGY

This chapter of the thesis covers the materials and methods used in the acquisition and processing of the data acquired.

4.1 Shallow seismic data acquisition

The equipment used to carry out the survey includes the following items; field notebook, tape measure, cutlass, ABEM Terraloc Mark 6 – 24 channel seismograph instrument, 24 geophones, seismic cables, 20 pound sledge hammer, 12 volt battery, metal plate, trigger switch and trigger cable and a personal computer for processing.

Figure 4.1: A picture of the ABEM terraloc seismograph equipment, cables and geophone.

The very first consideration in this seismic refraction survey was the geophone spacing. The spacing used depended on the depth of exploration and the details of the subsurface desired. As a rule of thumb, the length of a spread should be three to five times the maximum depth of interest (Redpath, 1973). The overlapping technique is used if the

length of the line was more than the length of the available cable. The general shot-detector setup is shown in figure 4.2.

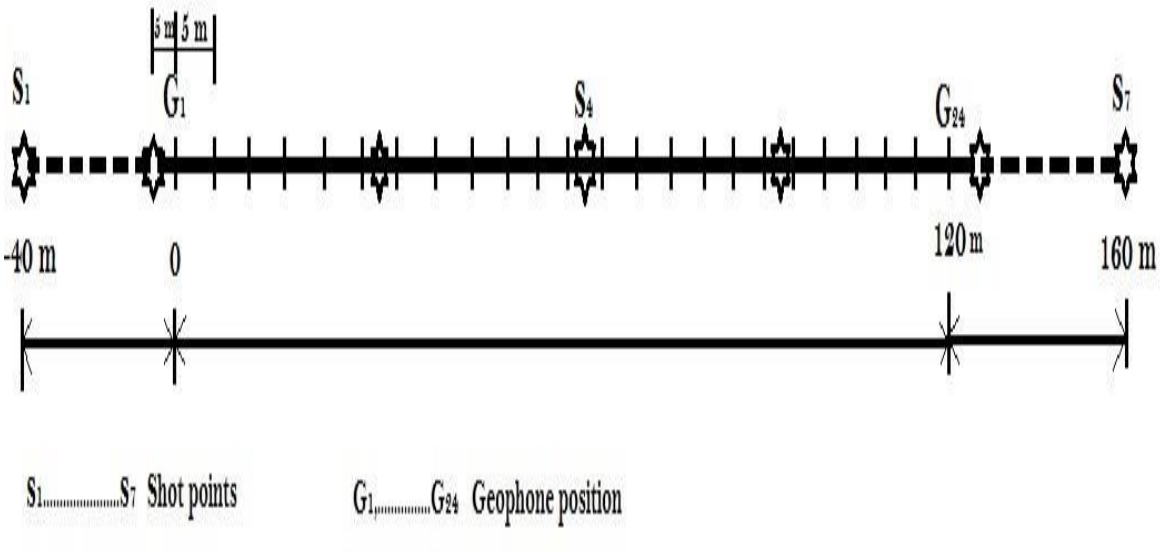

Figure 4.2: Source detector configuration, G1-G24 represents the geophones positions and S is the shot point

A total of ten profile lines with varying lengths had been planned for this survey site. The overlapping technique was used on lines longer than 115 m. For each spread, a total number of 24 geophones were used with separation intervals of either 4 or 5 m and a maximum of seven shot points. The details of each line is shown in table 4.1 The acquisition parameters set on the seismograph are stated in table 4.2

Table 4.1: Details of profile lines at the project site

Profile line	Length (m)	Spacing (m)	Offset Shot (m)	Overlapping
1	420	5	40	YES

2	730	5	40	YES
3	140	4	25	NO
4	140	4	25	NO
5	200	5	25	NO
6	640	5	40	YES
7	165	5	25	NO
8	205	5	_	NO
9	275	5	20	YES
10	270	5	_	YES

Table 4.2: Seismic acquisition parameters

Measurement	Standard
Stacking mode	Preview
Delay	9.975 ms
Record length	102.400 ms
Number of samples	4096
Sampling interval	25µs
Number of stack	3
Source	Hammer
Receiver type	Vertical geophone
Cut off frequency	48 Hz
Attenuation	12dB

The following describes the steps that were followed during the data collection stages of this research.The survey lines were marked and cleared. The sampling patterns in the survey plan were followed and the cables and geophones were setup.The seismograph was then set up and the geophones response tested. The metal plate and trigger geophone were placed at their designated points along the line.Several shots were conducted at each marked shot point using a sledge hammer and the integrity of the shot inspected.

The desired shot data was saved in SEG2 format.

The metal plate, hammer and trigger geophone were moved to the next shot point and the steps above repeated.

Figure 4.3: (A) Geophysicist setting up geophones (B) Setting the seismograph (C) Testing the geophones response (D) Shot about to be taken

4.2 Seismic data processing

The recorded data was processed with reflexW version 5 by Sandmeier, which interpretes the data using the intercept time method. One has to be extra careful when picking first breaks because noise recorded can be deceptive.

The 2D-data analysis module of reflex W was used to import the data.In situations where there were more than one spread for a single line, the following steps were carried out to combine them; within the fileheader coordinates segment of the 2D data analysis, the positions of the last two geophones in the first spread were set as the positions of the first two geophones in the next spread (figure 4.4). This system allows the entire profile line to

appear as a single line. The values of the shot positions were also adjusted to suit this new arrangement.

A bandpass frequency range of 17 MHz low-cut off and 300MHz high cut-off was used to filter the data representing each spread in order to reduce the level of noise.

Secondly, dewowing was applied to enhance the amplitudes of the first arrivals. The manual gain function was then applied to suppress the unwanted signals on the wiggles so as to reveal the first arrivals. Activating the picking possibilities, the first arrival times were picked using the manual pick mode and saved.

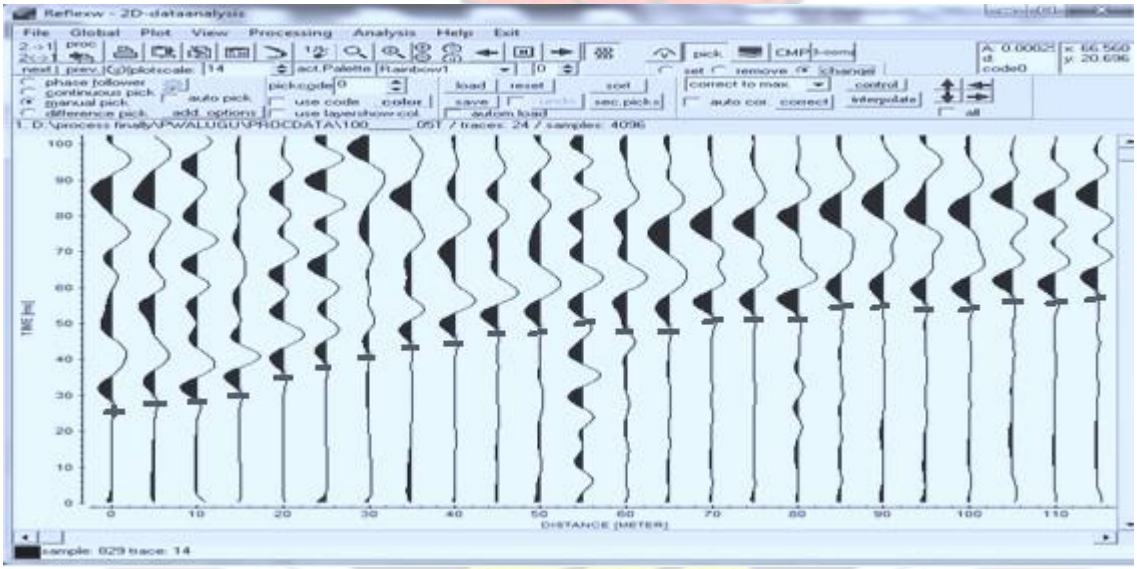

Figure 4.4: ReflexW window showing picked first arrivals.

Inversion of the travel time data were carried out in the traveltime analysis 2D module. The arrival times versus shot point-to-geophone distance were plotted.The reciprocal of the slopes of the time - distance segments gives the apparent seismic velocity of that layer of the earth.Similar line segments were picked and combined and later inverted directly using the wavefront inversion method into the underground model.

CHAPTER 5

RESULTS DISCUSSIONAND INTERPRETATIONS

This section elaborates on the results obtained on the field and their respective discussions.

5.1 Seismic refraction data analysis and interpretations

Seismic refraction data has several techniques for interpretations, these techniques depends on the character of the refractor. The techniques are mostly grouped into the following:

1. The intercept-time method (Barton and Barker 2003; Adachi, 1954; Hales 1958; Hagedoom, 1959),
2. The delay-time/reciprocal method (Wyrobek1956; Palmer 1980;Leung

   1995,1997, 2003; and Sjogren 2000)
3. Ray tracing method (Whitley 2002, 2004)
4. Seismic refraction tomography method (Hofman et al.,2003; Boschetti et al., 1996; Roach 2003; Sheehan et al.,2005;Wright 2006;).

The intercept-time method can mostly be done with a calculator and a pencil or with a spreadsheet program. The ray tracing method requires significant computational resources. The reciprocal method varies from simple to generalized versions that require microcomputers computers. The important information required to compute the thicknesses and seismic velocities of the near surface weathering layers which give the indication of the geological structure on this basis are provided by seismic surveys. The velocities of the layers delineated are the reciprocal of the slope of the curves. Both the direct and refracted curves were fitted and their slope and intercept times were calculated

using linear regression formulas in (equations22 and 24). The depth to the refractor beneath each detector is computed using equations27 and 28.

The velocity-depth models were generated using the combined travel-time curves of all the shot-points made on each profile line. The differences between the total forward and reverse travel times were less than 5ms; this revealed a good layer assignment in the generation of stratigraphic models underground. The true layer velocities were computed using the line of best fit. The refraction seismic survey revealed three layers showing the stratigraphy of the area (figure 5.1).

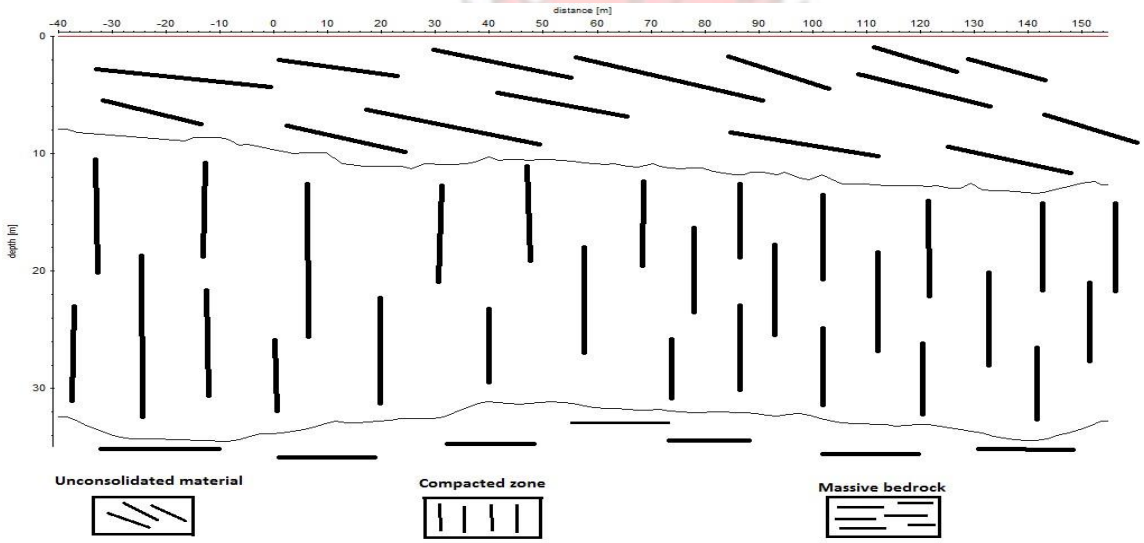

Figure 5.1 Stratigraphic model of study area.

5.1.1 Profile line 1

Three spreads were conducted along this profile line (420 m long) and a degree of overlapping of two geophones was employed.

The model associated with this line as shown in figure 5.2 reveals that, the subsurface to a depth of about 40 m is made up of three major layers with contrasting seismic

velocities.

The overburden has an average seismic velocity of 1400 m/s suggesting an unsaturated alluvium overburden. Its thickness ranges between 14and 22 m. The average apparent seismic velocity of the second layer is 2900 m/s indicating a compacted alluvium zone.

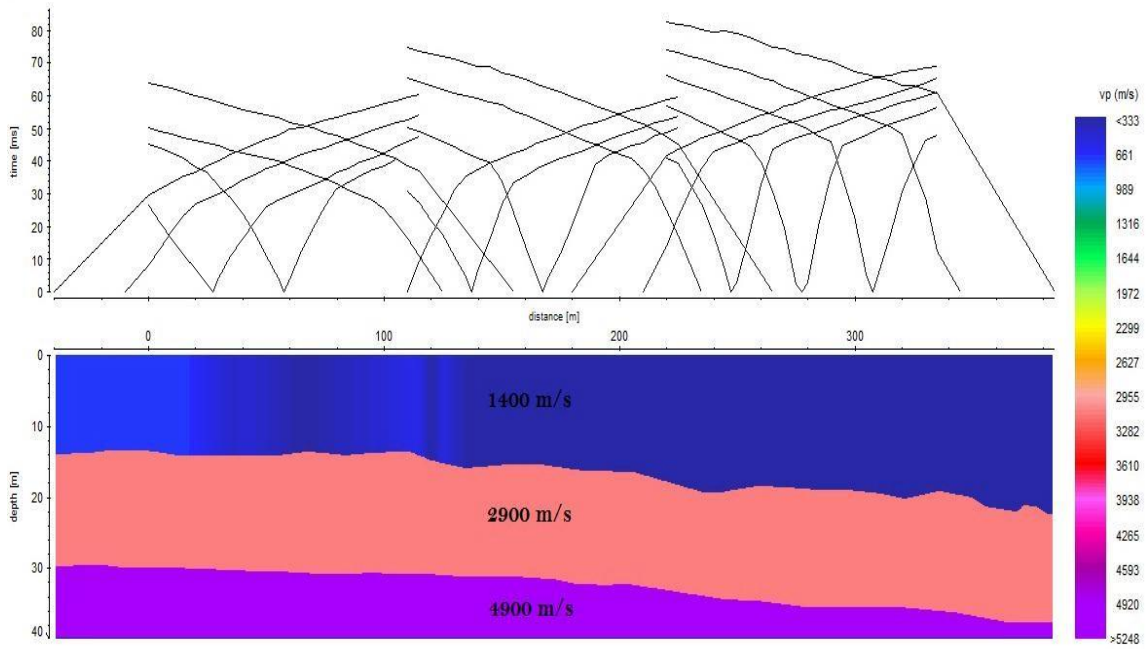

Figure 5.2 Time – distance graph and model of profile line_1

The thickness of this zone reaches a maximum value of about 16 m and this runs almost throughout the profile line. The third layer with a velocity of 4900 m/s is encountered at a minimum depth of 30 m. This velocity of this layer suggests sandstone bedrock and it dips towards the right hand side. The interpreted engineering properties of the seismic layers beneath this profile are illustrated in table 5.1

Table 5.1 Elastic constants of the layers encountered at profile line 1

Layer	V_P (m/s)	Poisson Ratio σ	Young's modulus E	Bulk modulus K (N/m^2)	Shear modulus μ (N/m^2)	Bulk density ρ (kg/m^3)

			(N/m^2)			
1	1400	0.25	3.1×10^9	2.1×10^9	1.24×10^9	1896
2	2900	0.25	15.9×10^9	10.6×10^9	6.38×10^9	2275
3	4900	0.25	51.9×10^9	34.6×10^9	20.8×10^9	2594

5.1.2 Profile line 2

A total distance of about 730 m was surveyed using six spreads and the overlap technique.

The model generated for this line shows three main layers (figure 5.3). The topmost layer with an average velocity of 1200 m/s is inferred to be an unconsolidated alluvium material. This layer has a maximum thickness of 12 m. The second layer is composed of materials with an average seismic velocity of 2900 m/s signifying saturated alluvium with a maximum thickness of about 26m. The third layer which is attributed to massive bedrock has an average seismic velocity of 4700 m/s. The bedrock is shallow at distances between 420 m mark and the end of the line.

The illustration in table 5.2 shows the elastic moduli of the seismic layers for this profile line.

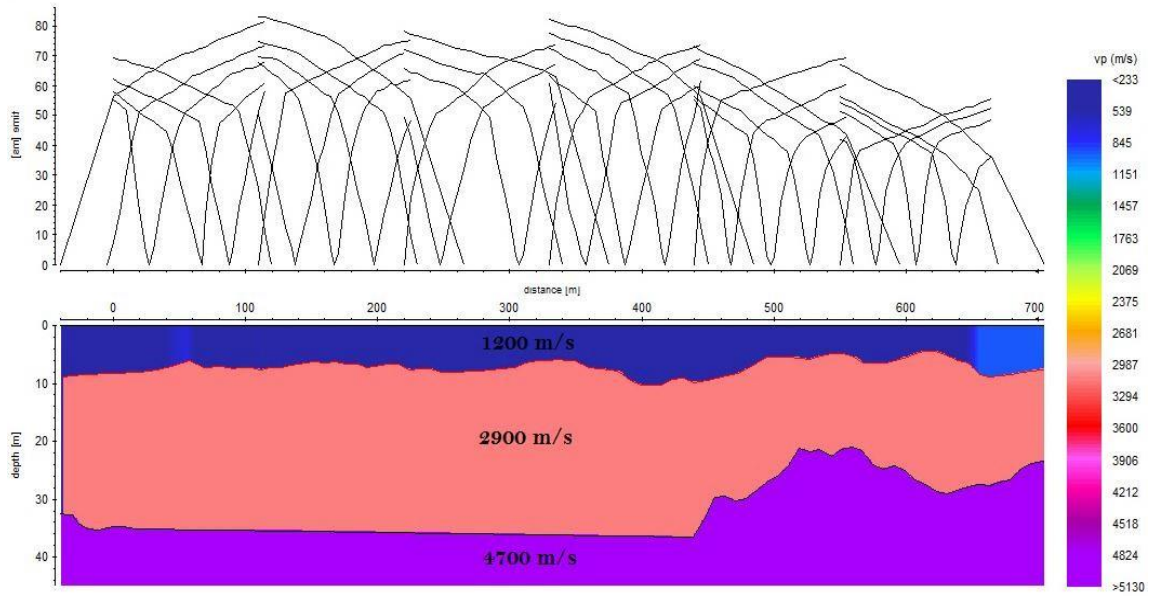

Figure 5.3 Time – distance graph and model of profile line 2

Table 5.2 Engineering properties of seismic layers for profile line 2

Layer	V_P (m/s)	Poisson Ratio σ	Young's modulus E (N/m^2)	Bulk modulus K (N/m^2)	Shear modulus μ (N/m^2)	Bulk density ρ (kg/m^3)
1	1200	0.25	2.2×10^9	1.5×10^9	0.9×10^9	1825
2	2900	0.25	15.9×10^9	10.6×10^9	6.4×10^9	2275
3	4700	0.25	47.2×10^9	31.5×10^9	18.9×10^9	2567

5.1.3 Profile line 3

The model associated with this line of 140 m length (figure 5.4) revealed that, the subsurface is made up of three major layers with contrasting seismic velocities. The overburden has varying seismic velocities with 1300 m/s as the average velocity, suggesting an unsaturated alluvium overburden with the thickness ranging between 7and 14 m along the profile. The average apparent seismic velocity of the second layer is 2600 m/s indicating a compacted alluvium zone.

Table 5.3 Engineering properties of seismic layers for profile line 3

Layer	V_P (m/s)	Poisson Ratio σ	Young's modulus E (N/m^2)	Bulk modulus K (N/m^2)	Shear modulus μ (N/m^2)	Bulk density ρ (kg/m^3)
1	1300	0.25	2.6×10^9	1.8×10^9	1.1×10^9	1861
2	2600	0.25	12.5×10^9	8.3×10^9	5.0×10^9	2214
3	4600	0.25	45.0×10^9	30.0×10^9	18.0×10^9	2553

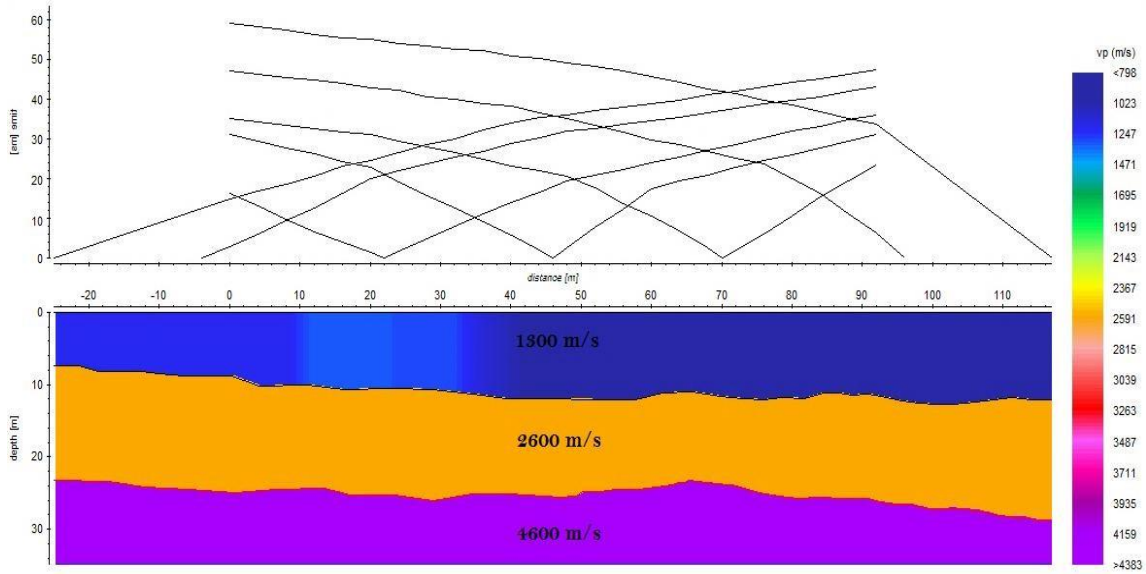

Figure 5.4 Travel time – distance graph and corresponding model of profile line 3 The third layer with a velocity of 4600 m/s is encountered at a minimum depth of 23 m. The velocity of the third layer suggests sandstone bedrock. The interpreted engineering properties of the seismic layers beneath this profile are illustrated in table 5.3 above

5.1.4 Profile line 4

This profile length of 140 m reveals three main layers with contrasting seismic velocities(figure 5.5). The topmost layer has an average velocity1000 m/s suggesting an unconsolidated alluvium material. The maximum thickness is about 15 m and it is seen in the middle of the line. The second layer is composed of materials with an average seismic

velocity of 1800 m/s signifying a compacted alluvium and its thickness increases to about 20 m towards the end of the line. The third layer, attributed to massive bedrock has an average of 3800 m/s. It is encountered at a minimum depth of 24 m and it dips to a maximum depth of 36 m along the profile.

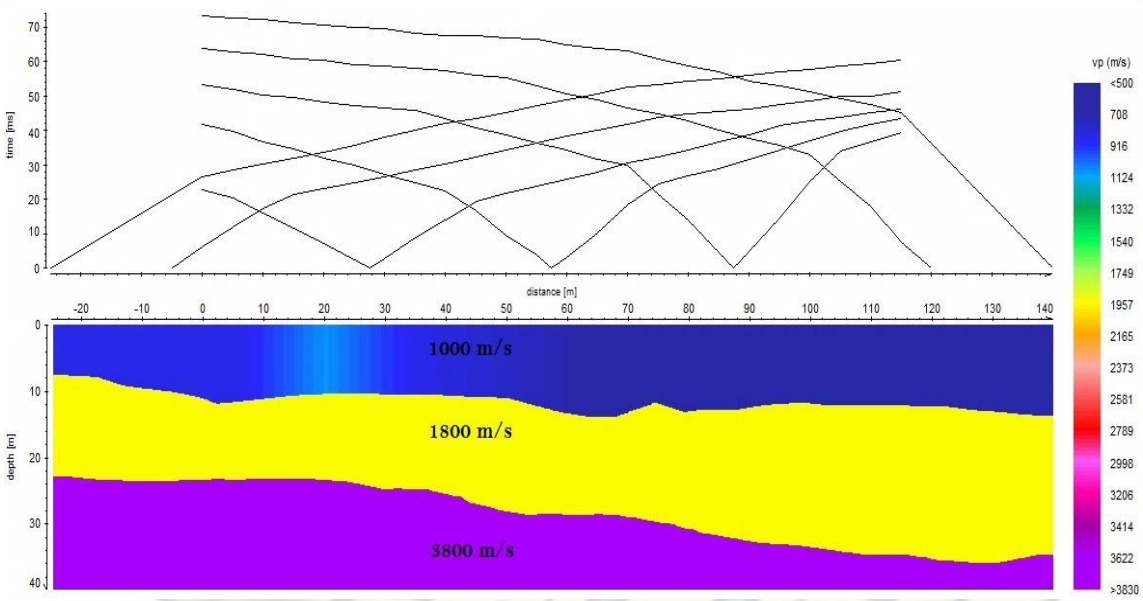

Figure 5.5 Travel time – distance graph and corresponding model of profile line 4

The bulk modulus of the bedrock is about $19 \times 10^9 \mathrm{N/m^2}$ as illustrated in table 5.4. **Table 5.4 Engineering properties of seismic layers for profile line 4**

Layer	V_P (m/s)	Poisson Ratio σ	Young's modulus E ($\mathrm{N/m^2}$)	Bulk modulus K ($\mathrm{N/m^2}$)	Shear modulus μ ($\mathrm{N/m^2}$)	Bulk density ρ ($\mathrm{kg/m^3}$)
1	1000	0.25	1.5×10^9	0.9×10^9	0.6×10^9	1743
2	1800	0.25	5.5×10^9	3.6×10^9	2.2×10^9	2019
3	3800	0.25	29.3×10^9	19.5×10^9	11.7×10^9	2434

5.1.5 Profile line 5

The associated model for this 200 m profile line as shown in figure 5.6 reveals that, the overburden has varying velocities with an average of 1200m/s, suggesting an unconsolidated alluvium.

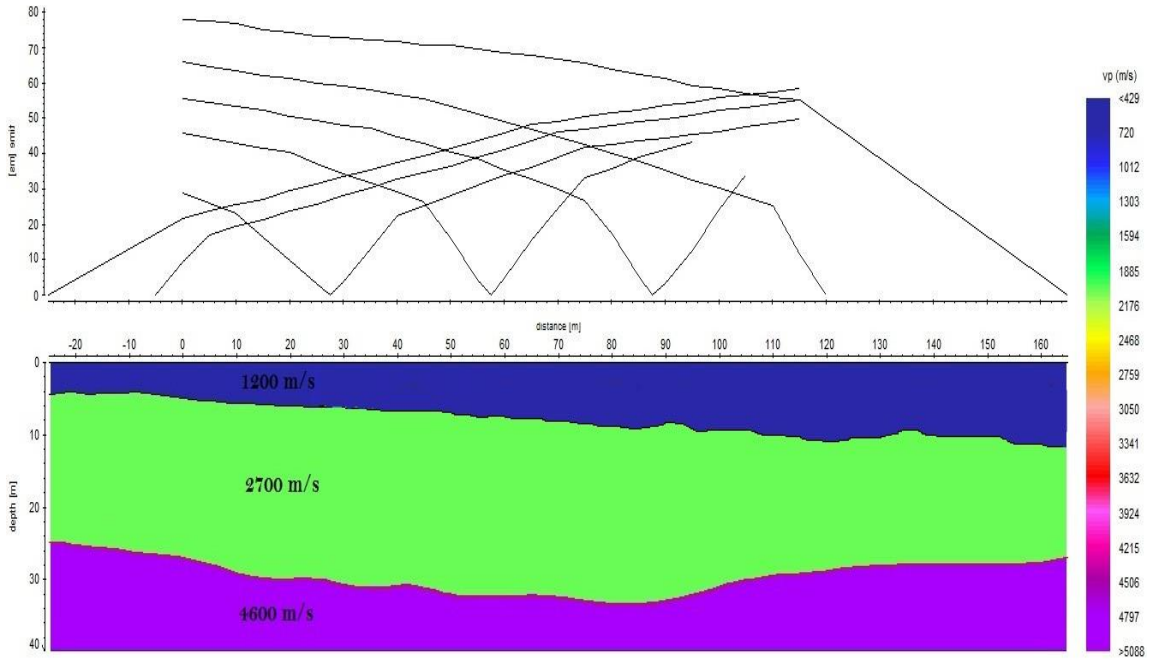

Figure 5.6 Travel time – distance graph and corresponding model of profile line 5

The next layer below has an average apparent velocity of 2700 m/s suggesting a compacted alluvium layer. On the average, the depth to this layer is between 6and 15 m. The third layer has an average seismic velocity of 4600 m/s resulting in a bulk density of 2553 kg/m^3 as indicated in table 5.5. This third layer suggests sandstone bedrock and it is depressed around the center.

Table 5.5 Engineering properties of seismic layers for profile line 5

Layer	V_P (m/s)	Poisson Ratio σ	Young's modulus E (N/m^2)	Bulk modulus K (N/m^2)	Shear modulus μ (N/m^2)	Bulk density ρ (kg/m^3)
1	1200	0.25	2.2×10^9	1.5×10^9	0.9×10^9	1825
2	2700	0.25	13.6×10^9	9.1×10^9	5.4×10^9	2234
3	4600	0.25	45.0×10^9	30.0×10^9	18.0×10^9	2553

5.1.6 Profile line 6

A total distance of about 640 m was measured using five spreads.

The model generated for this line (figure 5.7) shows three layers with contrasting seismic velocities. The overburden has an average velocity of 1300 m/s suggesting an unconsolidated material. This layer suggests an alluvium deposit with a maximum thickness of 12 m**.**

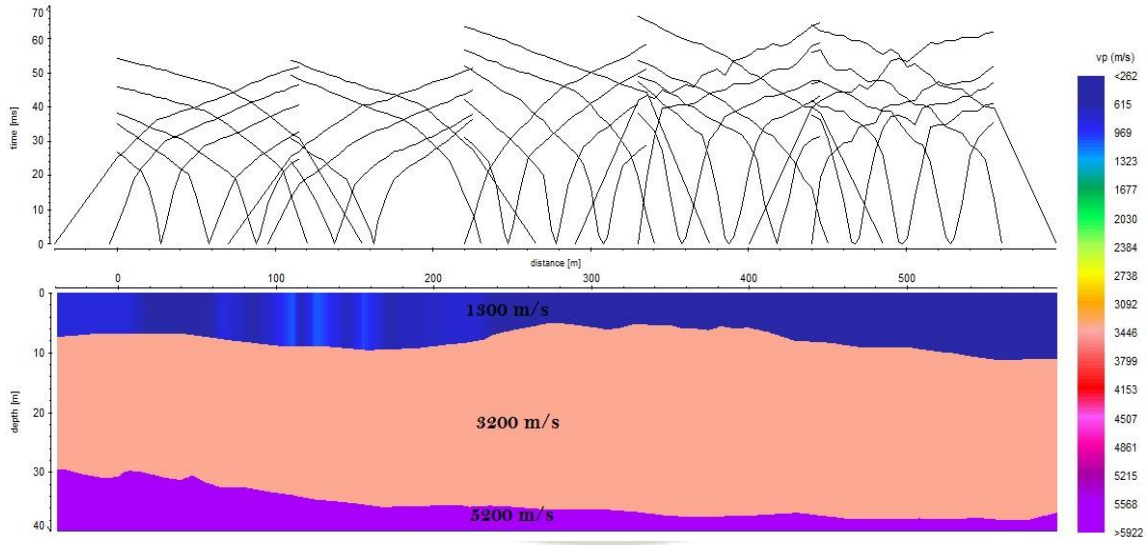

Figure 5.7 Travel time – distance graph and corresponding model of profile line 6.

Table 5.6 Engineering properties of seismic layers for profile line 6

Layer	V_P (m/s)	Poisson Ratio σ	Young'smodulus N/m^2 E ( )	Bulk N/m^2 modulus K ( )	Shear N/m^2 modulus μ ( )	Bulk kg/m^3 density ρ ( )
1	1300	0.25	2.6×10^9	1.75×10^9	1.1×10^9	1861
2	3200	0.25	19.9×10^9	1.33×10^9	8.0×10^9	2332
3	5200	0.25	59.3×10^9	39.5×10^9	23.7×10^9	2632

The second layer is composed of materials with an average seismic velocity of 3200 m/s which signifies a compacted alluvium with a maximum thickness of about 26 m.

The third layer which is attributed to massive bedrock has an average seismic velocity of 5200 m/s and has a dipping interface. The elastic properties of the layers are illustrated in table 5.6.

5.1.7 Profile line 7

A total length of 165 m was surveyed for this line and the associated model in figure 5.8 reveals that, the overburden suggests an unconsolidated alluvium with an average seismic velocity of 1100 m/s. The thickness ranges between 6and 8 m.

The consolidated layer with an average velocity of 2000m/s is encountered at a minimum depth of 6m and a maximum depth of about 8 m. The inferred sandstone bedrock has velocity of about 4500 m/s and it is encountered at a minimum depth of about 19 m. These rock layers encountered have the engineering properties shown in table 5.7.

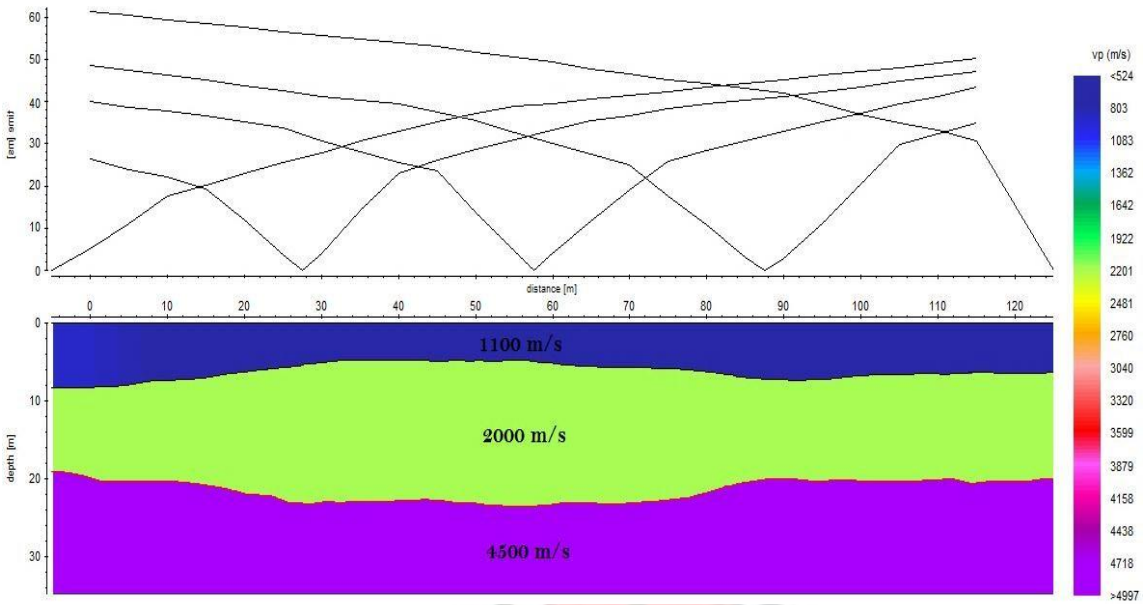

Figure 5.8 Travel time – distance graph and corresponding model of profile line 7

Table 5.7 Engineering properties of seismic layers for profile line 7

Layer	V_P (m/s)	Poisson Ratio σ	Young'smodulus E (N/m^2)	Bulk modulus K (N/m^2)	Shear modulus μ (N/m^2)	Bulk density ρ (kg/m^3)
1	1100	0.25	1.8×10^9	1.2×10^9	0.7×10^9	1785
2	2000	0.25	6.9×10^9	4.6×10^9	2.8×10^9	2073
3	4500	0.25	42.8×10^9	28.6×10^9	17.1×10^9	2539

5.1.8 Profile line 8

A total distance of about 205 m was measured and the model in figure 5.9 reveals that the overburden has an average velocity of 1300 m/s. The low velocity value suggests it is unconsolidated. The layer has a varying thickness ranging between 8 m and 10 m.

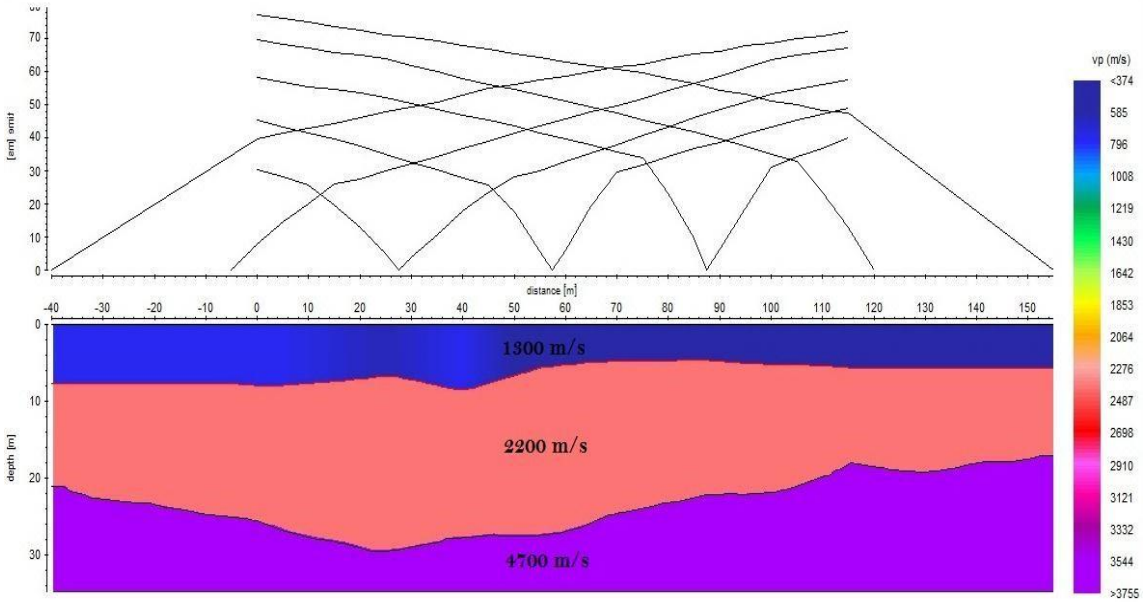

Figure 5.9 Travel time – distance graph and corresponding model of profile line 8

A relatively hard layer was encountered at depths beyond 10 m and is inferred to be the compacted alluvium zone, the measured average seismic velocity is about 2200 m/s. **Table 5.8 Engineering properties of seismic layers for profile line 8**

Layer	V_P (m/s)	Poisson Ratio σ	Young's modulus E (N/m^2)	Bulk modulus K (N/m^2)	Shear modulus μ (N/m^2)	Bulk density ρ (kg/m^3)
1	1300	0.25	2.6×10^9	1.8×10^9	1.1×10^9	1861
2	2200	0.25	8.6×10^9	5.7×10^9	3.4×10^9	2123
3	4700	0.25	47.2×10^9	31.5×10^9	18.9×10^9	2567

The sandstone bedrock having average velocity of 4700 m/s is encountered at depths ranging from 19 m and beyond. Table 5.8 illustrates the elastic constants of the encountered layers.

5.1.9 Profile line 9

The model associated with this profile (275 m long)as shown in figure 5.10 revealed that, the subsurface is made up of three major layers with contrasting seismic velocities.

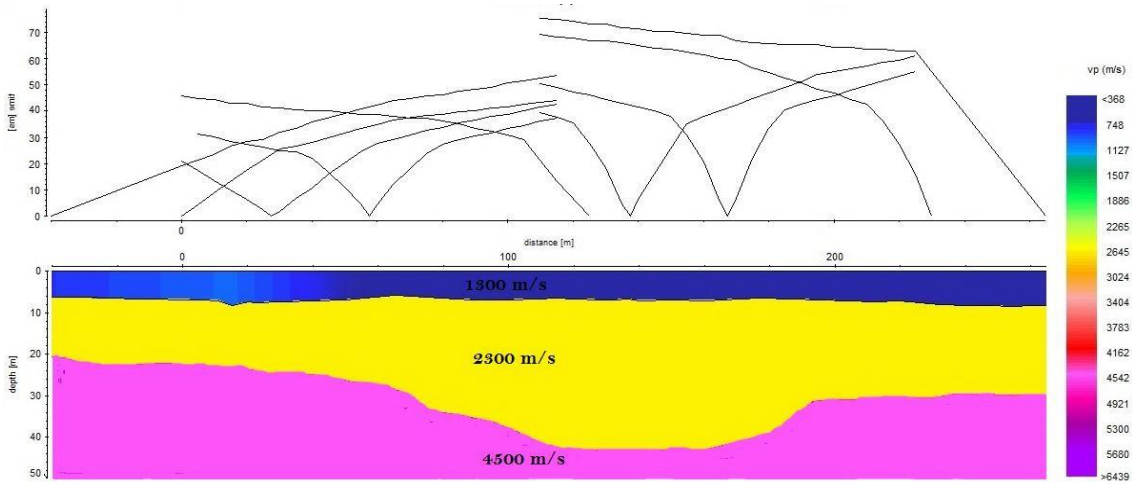

Figure 5.10 Travel time – distance graph and corresponding model of profile line 9.

The overburden has varying seismic velocities with 1300 m/s as the average seismic velocity, suggesting an unsaturated alluvium overburden. The thickness ranges between 8and 10 m along the profile. The average apparent seismic velocity of the second layer is 2300 m/s indicating a compacted alluvium zone.

Table 5.9 Engineering properties of seismic layers for profile line 9

Layer	V_P (m/s)	Poisson Ratio σ	Young's modulus E (N/m^2)	Bulk modulus K (N/m^2)	Shear modulus μ (N/m^2)	Bulk density ρ (kg/m^3)
1	1300	0.25	2.6×10^9	1.75×10^9	1.05×10^9	1861
2	2300	0.25	9.5×10^9	6.3×10^9	3.79×10^9	2147
3	4500	0.25	42.8×10^9	28.6×10^9	17.1×10^9	2539

The third layer with a velocity of 4500 m/s is encountered at a minimum depth of 20 m. This layer suggests sandstone bedrock. The bedrock dips to the right and has a depression in its center. The interpreted engineering properties of the seismic layers are illustrated in table 5.9

5.1.10 Profile line 10

The profile line covered a distance of 270 m and the model associated with it as shown in figure 5.11 revealed that, the subsurface to a depth of about 45 m is made up of three major layers with contrasting seismic velocities.

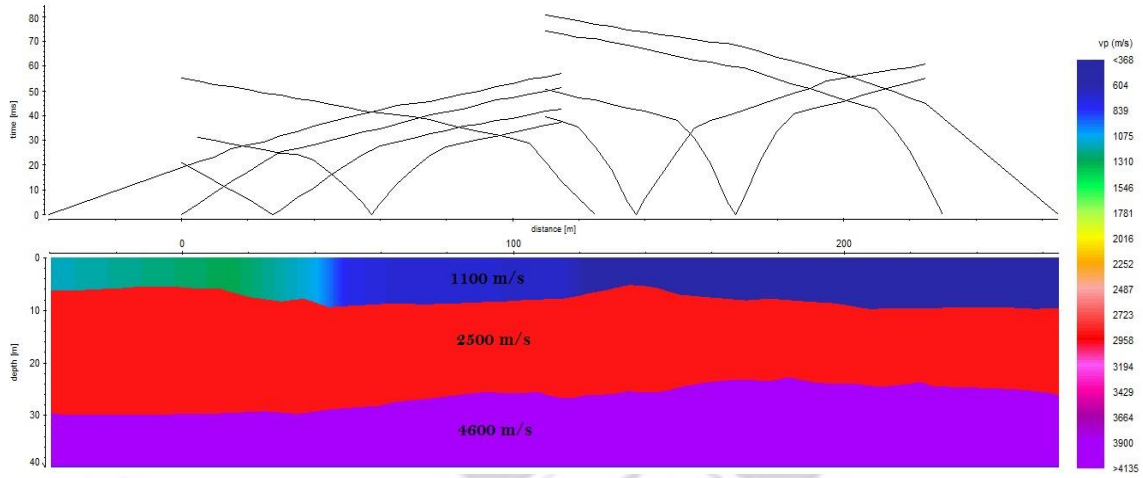

Figure 5.11 Travel time – distance graph and corresponding model of profile line 10

Table 5.10 Elastic constants of seismic layers for profile line 10

Layer	V_P (m/s)	Poisson Ratio σ	Young's modulus E (N/m^2)	Bulk modulus K (N/m^2)	Shear modulus μ (N/m^2)	Bulk density ρ (kg/m^3)
1	1100	0.25	1.8×10^9	1.2×10^9	0.72×10^9	1785
2	2500	0.25	11.4×10^9	7.6×10^9	6.38×10^9	2192
3	4600	0.25	45.0×10^9	30.0×10^9	20.8×10^9	2553

The overburden has varying seismic velocities and its average is 1100 m/s suggesting an unsaturated alluvium overburden with a maximum thickness of 9 m. The average apparent seismic velocity of the second layer was estimated to be 2500 m/s indicating a compacted alluvium zone. This layer is thick at the start of the line and gradually thins towards the end.

The third layer which is attributed to massive bedrock has an average seismic velocity of 4600 m/s and is first encountered at a minimum depth of about 26 m. The calculated elastic properties of the bedrock have a shear modulus of $20.8 \times 10^9\ \mathrm{N/m^2}$ as illustrated in table 5.10 above.

CHAPTER 6

CONCLUSION AND RECOMMENDATIONS

6.1 Conclusion

The seismic refraction survey technique was carried out at the proposed site to investigate the subsurface and delineate features so as to ascertain if the foundation can support the dam. This work was also to determine the number of distinct seismic layers within a depth of about 40m and their respective thicknesses. The elastic properties of the layers were also estimated using the respective layer velocities. The data acquired were inverted into velocity- depth models using the intercept time method.

The velocity sections show that shallow subsurface of Pwalugu is dominated by three layers with distinct velocity levels. The lower velocities (up to 1400m/s) correspond to alluvium and filling material cover at the site. The second layer with intermediate velocities between 2000 to 3200 m/s is associated with saturated alluvium with thickness ranging between 12 and 30 m. The third layer with relatively high velocities between3200 to 5200m/s is associated with the sandstone bedrock. Most of the sandstone bed lies beyond a depth of 20 m whilst the overburden is mostly less than 19 m in thickness. The bedrock is dipping and some cases and in some other instances it has depressions giving it high depths at those points. No faults had been detected in the bedrock in all the ten profile lines. The maximum depth to the massive bedrock is about 42 m. The average values of the Young, Bulk, Shear modulus and Bulk Densities corresponding to the three layers are shown in table 6.1 below.

The high average seismic velocity of the bedrock and the associated high elastic constants suggests that the third layer is the strongest. When the elastic constants of the bedrock is compared with the ranges for intact sandstone (table 6.2), it can be deduced that the

bedrock is in very reliable physical state and can therefore support the dam. **Table 6.1 Range of some elastic constants for intact sandstone**

Shear modulus (N/m^2)	**Bulk modulus**(N/m^2)	**Young modulus**(N/m^2)
$1.2 - 41.6 \times 10^9$	$1.8 - 111 \times 10^9$	$3.24 - 99.9 \times 10^9$

Table 6.2Average Elastic Moduli and densities of seismic layers at the site

Layer	**Young modulus E** (N/m^2)	**Bulk modulus K** (N/m^2)	**Shear modulus μ** (N/m^2)	**Bulk density** ρ (kg/m^3)
1	2.3×10^9	1.55×10^9	0.94×10^9	1830
2	11.97×10^9	6.77×10^9	4.97×10^9	2188
3	45.55×10^9	30.38×10^9	20.8×10^9	2553

6.2 Recommendations

The electrical resistivity tomography as well as seismic refraction tomography can be used to study the sites so as to verify the findings made in this research.

In the event of the siting of a huge engineering structure, the depth to about 42 m should be used so that the foundation of the structure will be properly supported.

REFERENCES

1. Adachi R (1954). On a proof of fundamental formula concerning refraction method of geophysical prospecting and some remarks. *Kumamoto J Sci. 2*(1):18–23

2. Alhassan, D. U., Dangana, L.M., Salako, K.A., Jonah, S.A. and Ofor, N.P.(2010)Seismic Refraction Investigation Of The Subsurface Structure At The Southern Part Of Niger State College Of Education, Minna, Nigeria. Bayero Journal Of Pure And Applied Sciences, 3(2): 56 - 61

3. Al-Saigh, N. H., & JaddoaAl-Heety, A. (2014). Seismic RefractionTomography and MASW Survey for Geotechnical Evaluation of soil for the Teaching Hospital Project at Mosul University. Journal of Zankoy Sulaimani-Part A (JZS-A), 16(1), 1.

4. Andrews, N., Aning, A., Danuor, S., and Noye, R. (2013). Geophysical investigations at theproposed site of the knust teaching hospital building using 2d and 3d resistivity imaging techniques. Int. Res. Jour. Geol. Min, 3(3):113–123.84

5. Barton, P., & Barker, N. (2003). Velocity imaging by tau–p transformation of refracted seismic traveltimes. *Geophysical Prospecting*, *51*(3), 195-203.

6. Begg, G. C., Griffin, W. L., Natapov, L. M., O'Reilly, S. Y., Grand, S. P., O'Neill, C. J., ... & Bowden, P. (2009). The lithospheric architecture of Africa: Seismic tomography, mantle petrology, and tectonic evolution. Geosphere, 5(1), 23-50.

7. Bekler, T. E. (2011). Characterization of a Landslide using Seismic Refraction, Electrical Resistivity and Hydrometer Methods, Adatepe—Çanakkale, NW Turkey. Journal of Environmental & Engineering Geophysics, 16(3), 115-126.

8. Benson, R., Glaccum, R. A., and Noel, M. R. (1984). Geophysical techniques for sensing buried wastes and waste migration. In Geophysical techniques for sensing buried wastes and waste migration. EPA.

9. Benson, R. C. and Yuhr, L. (1995). Geophysical methods for environmental assessment. In Geoenvironment 2000@ sCharacterization, Containment, Remediation, and Performance in Environmental Geotechnics, pages 57–76. ASCE.

10. Benson, R. and Yuhr, L. (2002). Site characterization strategies: old and new. In Second Annual Conference on the Application of Geophysical and NDT Methodologies to Transportation Facilities, Federal Highway Ad-ministration, April, pages 15–19.

11. Boschetti, F., Dentith, M. C., & List, R. D. (1996). Inversion of seismic refraction data using genetic algorithms. *Geophysics*, *61*(6), 1715-1727.

12. Castle Minerals Pty Ltd. (2012, 06). http://www.castleminerals.com/background.php. Retrieved 04 19, 2014

13. Cecil, OS (1971). Correlation of seismic refraction velocities and rock support requirementsin Swedish tunnels. Swedish Geotechnical Inst Reprints & Repts.

14. Delgado, J., Casado, C. L., Estevez, A., Giner, J., Cuenca, A., & Molina, S. (2000a). Mapping soft soils in the Segura river valley (SE Spain): a case study of microtremors as an exploration tool. *Journal of Applied Geophysics*, *45*(1), 19-32.

15. Delgado J, Lopez C C, Giner J, Estevez A, Cuenca A and Molina S 2000b Microtremors as a geophysical exploration tool: applications and limitations *Pure Appl. Geophys.* **157** 1445–62

16. Delgado J, Alfaro P, Galindo-Zaldivar J, Jabaloy A, Lopez Garrido A C and Sanz De Galdeano C 2002 Structure of the Padul-Niguelas Basin (S Spain) from H/V ratios ofambient noise: application of the method to study peat and coarse sediments Pure Appl. Geophys. 159 2733–49

17. Doblas, M., López-Ruiz, J., Cebriá, J. M., Youbi, N., & Degroote, E. (2002). Mantle insulation beneath the West African craton during the Precambrian-Cambrian transition. Geology, 30(9), 839-842.

18. Dutta, N. (1984). Seismic refraction method to study the foundation rock of a dam. Geophysical prospecting, 32(6):1103–1110.

19. East Mamprusi District, 2014. Retrieved sep 2014, from http://www.eastmamprusi.ghanadistricts.gov.gh/

20. El-Aal, A. A., & Mohamed, A. A. (2010). Near-surface seismic refraction applied to exploring subsurface clay layer at a new mining area in southeast Cairo, Egypt. Arabian Journal of Geosciences, 3(2), 105-112.

21. en.wikipedia.org/wiki/West_Africa_Craton. (26 12, 2010). Retrieved 04 18, 2014

22. GGS. (2009). Geological Map of Ghana; Database of Ghana Geological Survey. Technical.

23. Goldstein, N. E. (2009). Expedited site characterization geophysics: geophysical methods and tools for site characterization.

24. Haeni, F. P. (1988). Application of seismic-refraction techniques to hydrologic studies. US Government Printing Office.

25. Hagedoorn, J. G. (1959). THE PLUS_MINUS METHOD OF INTERPRETING SEISMIC REFRACTION SECTIONS*. *Geophysical prospecting*, *7*(2), 158-182.

26. Hales, F. W. (1958). An accurate graphical method for interpreting seismic refraction lines. *Geophysical prospecting*, *6*(3), 285-294.

27. Hatherly, PJ., &Neville, M. (1986). Experience with the generalized reciprocal method of seismic refraction interpretation for shallow engineering site investigation. Geophysics, 51(2):255–265.

28. Hofmann T., &Schrott, L. (2003). Determining sediment thickness of talusslopes and valley fill deposits using seismic refraction- a comparison of 2D interpretation tools (with 7 figures and 3 tables). ZEITSCHRIFT FUR GEOMORPHOLOGIE SUPPLEMENTBAND, 71-87.

29. Ibs-von Seht, M., & Wohlenberg, J. (1999). Microtremor measurements used to map thickness of soft sediments. *Bulletin of the Seismological Society of America*, *89*(1), 250-259.

30. Ilesanmi, O. M., Oladapo, A., Olanike, O., Foluwaso, A., Oluseun, B., & William, I. (2013). Seismic refraction study of Gurara dam phase II, northwestern Nigeria.

31. Keary, P., Brooks, M., & Hill, I. (2002). An introduction to geophysical exploration. Blackwell Science Ltd.

32. Kesse, G. O. (1985). The mineral and rock resources of Ghana.

33. Kilty, K.T., Norris, R. A., McLamore, W.R., Hennon, K. P., & Euge, K. (1986). Seismic refraction at Horse Mesa Dam: An application of the generalized reciprocal method. Geophysics, 51(2), 266-275.

34. Khan, M. Y. (2013). Engineering geophysical study of unconsolidated top soil using shallowseismic refraction & electrical resistivity techniques. Journal of Environment & Earth Science, 3(8):120–127.

35. Lanz, E., Maurer, H., & Green, A. G. (1998). Refraction tomography over a buried waste disposal site. Geophysics, 63(4), 1414-1433

36. Leung, T. M. (1995). Examination of the optimum XY value by ray tracing.*Geophysics*, *60*(4), 1151-1156.

37. Leung, T. M. (1997). Evaluation of seismic refraction interpretation using first arrival raytracing. *Geological Society, London, Engineering Geology Special Publications*, *12*(1), 413-416.

38. Leung, T. M. (2003). Controls of traveltime data and problems of the generalized reciprocal method. *Geophysics*, *68*(5), 1626-1632.

39. Leube, A. H. (1990). The early proterozoic Birimian supergroup of Ghana and some aspects of its associated gold mineralisation . Precambrian Research, 46, 139-165.

40. Milsom, J. (2007). *Field geophysics* (Vol. 25). John Wiley and Sons.

41. Mooney, H. M. (1980). Handbook of engineering geophysics (Vol. 1). Bison Instruments

42. Mooney, B. K., (1984), ―Reduction Scheme in Seismic Refraction‖, Musgrave Company, U.S.A, 322 – 356.

43. Moustafa, S.S.,Ibrahim,E.H.,Elawadi, E., Metwaly, M., and Al Agami, N (2012). Seismic refraction and resistivity imaging for assessment of groundwater seepage

under a dam site, southwest of saudi arabia. International Journal of Physical Sciences, 7(48):6230-6239.

44. Palmer D (1980) The generalized reciprocal method of seismic refraction interpretation. In: Burke KBS (ed) Soc Explor Geophys, p 101

45. Parolai S, Borman P and Milkreit C 2001 Assessment of the naturalfrequency of the sedimentary cover in the Cologne area(Germany) using noise measurements J. Earthq. Eng. 5 541–64

46. Parolai S, Borman P and Milkreit C 2002 New relationshipsbetween Vs, thickness of sediments and resonance frequencycalculated by H/V ratio of seismic noise for the Cologne area(Germany) Bull. Seismol. Soc. Am. 92 2521–7

47. Rao, V. V., Raju, J. S., Rao, B. P., & Rao, P. K. (2004). Bedrock investigation by seismic refraction method–A case study. J. Ind. Geophy. Union, 8(3), 223-228.

48. Redpath, B. B. (1973). Seismic refraction exploration for engineering site investigations. Explosive Excavation Research Laboratory Livermore, California: National Technical Information Service.

49. Reynolds, J. M. (1997). An Introduction to Applied And Environmental Geophysics. Chichester: John Wiley & Sons Ltd.

50. Roach I C (2003) Advances in Regolith. Proceedings of the CRCLEME Regional Regolith Symposia, 2003

51. Rucker, M. L. (2000). Applying the seismic refraction technique to exploration for transportation facilities. Geophysics, 1:1–3.

52. Sandmeier, J.K (2008). Reflex W V-5 manual: Windows (9x/NT/2000/XP-program for the processing of seismic, acoustic or electromagnetic reflection, refraction and transmission data.

53. Schlüter, T. (2006). Geological Atlas of Africa. Geological Atlas of Africa, With Notes on Stratigraphy, Tectonics, Economic Geology, Geohazards and Geosites of Each Country. by T. Schlüter. 2006 XII, 272 p., 249 illus. With CD-ROM. 3-54029144-X. Berlin: Springer, 2006., 1.

54. scribd.com. (2013). Retrieved Feb 09, 2014, from http://www.scribd.com/doc/168791372/Lecture-2-Seismic-Refraction-Methods.

55. SEG. (2014). Retrieved 01 25, 2014 from www.seg.org/education/youthresources/what-is-geophysics.

56. Sheehan, J. R., Doll, W. E., & Mandell, W. A. (2005). An evaluation of methods and available software for seismic refraction tomography analysis. *Journal of Environmental & Engineering Geophysics*, *10*(1), 21-34.

57. Sheriff, R. E., &Geldart, L. P. (1995). *Exploration seismology*. Cambridge university press.

58. Soupios, P. M., Georgakopoulos, P., Papadopoulos, N., Saltas, V., Andreadakis, A., Vallianatos, F., ... & Makris, J. P. (2007). Use of engineering geophysics to investigate a site for a building foundation. *Journal of Geophysics and Engineering*, *4*(1), 94.6

59. Spencer, A. C., (1973), ―Economic Geology‖ 17, 312 – 317.

60. Sjøgren, B., Øfsthus, A., and Sandberg, J. (1979). Seismic classification of rock massqualities*. Geophysical Prospecting, 27(2):409–442.

61. Sjögren, B. (2000). A brief study of applications of the generalized reciprocal method and of some limitations of the method. *Geophysical prospecting*, *48*(5), 815-834.u

62. Telford, W. M., Geldart, L.P., &Sheriff, R. E. (1990). Applied geophysics (vol. 1) Cambridgeuniversity press.

63. Ueblacker, H. (2006). Feasibility Level Geological and Geotechnical Investigation for Union Park Dam. In Golden Rocks 2006, The 41st US Symposium on Rock Mechanics (USRMS). American Rock Mechanics Association.

64. US Department of Transportation (2014). Determining the engineering properties of the subsurface. Central Fedral Lands Highway division Retrieved 27/09/2014 from http://www.cflhd.gov/favicon.ico

65. Ushie, F. A., (2010), ―Economic Evaluation of lateritic rocks in Obudu Area, Southeastern Nigeria‖, Ph.DThesis. Nnamdi Azikiwe University Awka, Nigeria

66. Varnes, D. (1978). Slope movements types and processes, schuster rl & krizek rjed.landslide, analysis and control. Transportation Research Board Sp. Rep, (176).

67. VRA Ghana (2013). Pwalugu Multipurpose Dam; Retreaved 07/08/2015 from http://www.vra.com/about_us/images/pmd_project_brochure.pdf

68. Whiteley R J (2002) Shallow refraction interpretation in complexconditions with visual interactive ray tracing: 64th EAGEConference & Exhibition, paper P155

69. Whiteley, R. J. (2004). Shallow seismic refraction interpretation with visual interactive ray trace (VIRT) modelling. *Exploration Geophysics*, *35*(2), 116-123.

70. Wright, C. (2006). The LSDARC method of seismic refraction analysis: principles, practical considerations and advantages. *Near Surface Geophysics*,*4*(3), 189-202.

71. Wright, J. B. (1986). Geology and mineral resources of West Africa. Springer Science & Business Media.

72. Wyrobek, S. M. (1956). Application of Delay and Intercept Times in the Interpretation of Multilayer Refraction Time Distance CURVES*. *Geophysical Prospecting*, *4*(2), 112-130.

73. Zohdy, A. A., Eaton, G. P., & Mabey, D. R. (1974). Application of surface geophysics to ground-water investigations. US Government Printing Office.